

CFD ANALYSES OF HEAT SINKS FOR CPU COOLING WITH FLUENT

A THESIS SUBMITTED TO
THE GRADUATE SCHOOL OF NATURAL AND APPLIED SCIENCES
OF
MIDDLE EAST TECHNICAL UNIVERSITY

BY

EMRE ÖZTÜRK

IN PARTIAL FULFILLMENT OF THE REQUIREMENTS
FOR
THE DEGREE OF MASTER OF SCIENCE
IN
MECHANICAL ENGINEERING

DECEMBER 2004

Approval of the Graduate School of Natural and Applied Sciences

Prof. Dr. Canan ÖZGEN
Director

I certify that this thesis satisfies all the requirements as a thesis for the degree of Master of Science.

Prof. Dr. Kemal İDER
Head of Department

This is to certify that we have read this thesis and that in our opinion it is fully adequate, in scope and quality, as a thesis for the degree of Master of Science.

Asst. Prof. Dr. İlker TARI
Supervisor

Examining Committee Members

Prof. Dr.Hafit YÜNCÜ	(METU, ME)	_____
Asst. Prof. Dr. İlker TARI	(METU, ME)	_____
Asst. Prof. Dr. Merve ERDAL	(METU, ME)	_____
Asst. Prof. Dr. Cüneyt SERT	(METU, ME)	_____
Dr. Ünver ÖZKOL	(ASELSAN)	_____

I hereby declare that all information in this document has been obtained and presented in accordance with academic rules and ethical conduct. I also declare that, as required by these rules and conduct, I have fully cited and referenced all material and results that are not original to this work.

Name, Last name: Emre ÖZTÜRK

Signature :

ABSTRACT

CFD ANALYSES OF HEAT SINKS FOR CPU COOLING WITH FLUENT

ÖZTÜRK, Emre

M.S. Department of Mechanical Engineering

Supervisor: Asst. Prof. Dr. İlker TARI

December 2004, 93 pages

In this study, forced cooling of heat sinks mounted on CPU's was investigated. Heat sink effectiveness, effect of turbulence models, effect of radiation heat transfer and different heat sink geometries were numerically analyzed by commercially available computational fluid dynamics softwares Icepak and Fluent. The numerical results were compared with the experimental data and they were in good agreement. Conjugate heat transfer is simulated for all the electronic cards and packages by solving Navier-Stokes equations. Grid independent, well converged and well posed models were run and the results were compared. The best heat sink geometry is selected and it is modified in order to have lower maximum temperature distribution in the heat sink.

Key Words: Forced Cooling of Electronic Devices, CPU Cooling, Computational Fluid Dynamics, Conjugate Heat Transfer, Heat Sink Improvement.

ÖZ

FLUENT YAZILIMI İLE ISI KUYULARININ HAD ANALİZLERİ

ÖZTÜRK, Emre

Yüksek Lisans, Makina Mühendisliği Bölümü

Tez Yöneticisi: Yrd. Doç. Dr. İlker TARI

Aralık 2004, 93 Sayfa

Bu çalışmada bilgisayar işlemcilerinin ısınmasını önlemek için kullanılan ısı kuyularının zorlamalı taşınım ile soğutulması incelenmiştir. Isı kuyusu etkinliği, türbülans modellerinin ve ısınmının ısı transferine etkileri, ısı kuyusu geometrilerinin farklılığı ticari hesaplamalı akışkanlar dinamiği yazılımları Icepak ve Fluent ile incelenmiştir. Hesaplamalı akışkanlar dinamiği sonuçları deneysel verilerle karşılatırılmıştır ve uyumluluk gözlenmiştir . Navier Stokes denklemleri çözümlerek hesaplama alanındaki elektronik kartlarda konjuge ısı transferi çözülmüştür. Sayısal ağdan bağımsız, ve yakınsayan modeller tutarlı sınır koşullarıyla analiz edilmiş ve sonuçlar karşılatırılmıştır. Karşılatırılan modellerden en iyisi seçilip geometrik deęişikliklerle daha etkin bir ısı kuyusu oluşturulmuştur.

Anahtar Kelimeler: Elektronik Cihazların Zorlamalı Soğutulması, İşlemci Soğutması, Hesaplamalı Akışkanlar Dinamiği (HAD), Konjuge Isı Transferi, Isı Kuyusu İyileştirmesi.

To ANOVA, the CFD company I have co-founded.

ACKNOWLEDGEMENTS

I wish to express my deepest gratitude to my supervisor Asst. Prof. Dr. İlker Tarı for his close guidance, inspiration and invaluable help throughout the study.

I wish to express my sincere appreciation to Asst. Prof. Dr. Merve Erdal for her precious comments on Chapter 2.

I am grateful to my colleague Yavuz Selim Kayseriliođlu for his practical help during the spell and format check of the thesis, his attention and care was beyond human capability.

Finally, I express my deepest gratitude to my family and lovely Gülce, for their continuous encouragement, understanding and support.

TABLE OF CONTENTS

PLAGIARISM.....	i
ABSTRACT.....	iv
ÖZ.....	v
ACKNOWLEDGEMENTS.....	vii
TABLE OF CONTENTS.....	viii
CHAPTER	
1. INTRODUCTION.....	1
1.1 System Constraints.....	2
1.2 Design Parameters.....	4
1.3 Other Parameters.....	9
1.4 Fan Selection.....	10
1.5 Thermal Interface Materials.....	13
1.6 Assumptions.....	14
1.7 Solution Approaches.....	16
2. CFD MODELS and EQUATIONS SOLVED.....	19
2.1 Pre-processing.....	19
2.2 Solver Execution.....	20
2.2.1 Governing Equations of Fluid Flow.....	20
2.2.2 Mathematical Model.....	22
2.2.3 Flow Configuration and Bounday Conditions.....	24
2.2.4 Governing Equations to be Solved.....	31
2.2.5 Parameters and Unknowns	34
3. RESULTS OF CFD ANALYSES.....	37
3.1 Sources of Errors at CFD Analysis.....	37
3.1.1 Discretization	39
3.1.2 Convergence Issues.....	42
3.1.3 Grid Independency.....	44
3.1.4 Turbulence Modelling.....	47
3.1.5 Radiation Effects.....	49

3.3	Temperature Distributions.....	52
3.2	Comparison with Experimental Data.....	58
4.	HEAT SINK DESIGN IMPROVEMENTS.....	60
4.1	Optimization Cases.....	60
4.2	Number of Fins.....	60
4.3	Heat Sink Material.....	62
4.4	Base Thickness.....	64
5.	CONCLUSIONS.....	65
	REFERENCES.....	68
	APPENDIX A Details of the model.....	71
	APPENDIX B Mesh Generation.....	74
	APPENDIX C Fluent Solver Details.....	82
	APPENDIX D Physical Models.....	90

LIST OF TABLES

Table 1.1 Fan noise levels.....	12
Table 1.2 Thermal resistances of thermal interface materials.....	14
Table 2.1 Interior conditions.....	29
Table 2.2 Fan conditions.....	30
Table 3.1 Maximum and minimum temperatures for the three heat sinks.....	54
Table 3.2 Rise above ambient temperature values.....	59
Table 3.3 Experimental and numerical results.....	59
Table 4.1 Maximum and minimum temperatures on modified heat sinks.....	61
Table D.1 Surface emissivities.....	93

LIST OF FIGURES

Figure 1.1 Heat sink design parameters.....	4
Figure 1.2 Bottom view of Swiftech 462-A.....	5
Figure 1.3 Thermal conductivities of common heat sink materials and possible candidates.....	6
Figure 1.4 Two heat sinks with different fin geometry.....	7
Figure 1.5 Examples of fluted heat sinks and wavy heat sinks.....	7
Figure 1.6 Exact modelling and lumped parameter modelling of fans.....	15
Figure 2.1 Computational domain.....	23
Figure 2.2 CPU Heat sink, chipset heat sink and AGP heat sink.....	23
Figure 2.3 Alpha CPU heat sink.....	24
Figure 3.1 Air flow direction shown on heat sink fan assembly.....	39
Figure 3.2 Temperature distributions for different discretization schemes.....	40
Figure 3.3 Reference line for temperature comparison of different upwinding schemes.....	41
Figure 3.4 Temperature plots on the reference line for upwinding schemes.....	41
Figure 3.5 Temperature distributions for different convergence criteria.....	43
Figure 3.6 Temperature plots on the reference line for convergence criteria.....	44
Figure 3.7 Zoom-in picture of different mesh resolutions.....	45
Figure 3.8 Temperature distributions for different cell numbers.....	46
Figure 3.9 Temperature plots on the reference line for two different grids.....	47
Figure 3.10 Temperature distributions for different turbulence models.....	48
Figure 3.11 Temperature plots for two turbulence models.....	49
Figure 3.12 Temperature distributions for radiation comparison.....	50
Figure 3.13 Reference line for temperature comparison of radiation.....	51
Figure 3.14 Temperature plots on the reference line for radiation	51
Figure 3.15 Temperature distributions on different heat sinks.....	52
Figure 3.16 Path lines for heat sinks Alpha, Coolermaster and Evercool.....	56
Figure 3.17 Velocity vectors for chipset heat sink.....	57

Figure 4.1 Three modified versions of Alpha heat sinks.....	60
Figure 4.2 Alpha heat sinks with fewer fins.....	61
Figure 4.3 Temperature plots on the reference line for the original heat sinks and the heat sinks with fewer fins.....	62
Figure 4.4 Temperature plots for heat sink material comparison.....	63
Figure 4.5 Temperature contours on the copper heat sink.....	63
Figure 4.6 Temperature plots for heat sinks with different base thicknesses.....	64
Figure B.1 Grid on computer chassis walls.....	74
Figure B.2 Mesh of components inside the cabinet except than the heat sinks...	75
Figure B.3 Surface grid on CPU heat sink.....	76
Figure B.4. Maximum and minimum angles in the cell.....	78
Figure B.5 Non-conformal grid interface.....	79
Figure C.1 Flow chart of the SIMPLE algorithm.....	83

CHAPTER 1

INTRODUCTION

All electronic equipment relies on the flow of and control of electrical current to perform a variety of functions. Whenever electrical current flows through a resistive element, heat is generated [1]. Regarding the appropriate operation of the electronics, heat dissipation is one of the most critical aspects to be considered when designing an electronic box. Heat generation is an irreversible process and heat must be removed in order to maintain the continuous operation [2]. With various degrees of sensitivity, the reliability and the performance of all electronic devices are temperature dependent. Generally the lower the temperature and the change of temperature with respect to time, the better they are [2]. Pure conduction, natural convection or radiation cool the components to some extent whereas today's electronic devices need more powerful and complicated systems to cope with heat. Therefore new heat sinks with larger extended surfaces, highly conductive materials and more coolant flow are keys to reduce the hot spots.

The performance criterion of heat sinks is the thermal resistance, which is expressed as the temperature difference between the electronic component and ambient per watts of heat load. It is expressed with units K/W. Today's electronic chips dissipate approximately 70 W maximum whereas this number will be multiples in the near future. The temperature differences from the heat sink surface to the ambient range from 10 °C to 35 °C according to the heat removal capability of the installed heat sink.

Heat sinks may be categorized into five main groups according to the cooling mechanism employed [3]:

- Passive heat sinks which are used generally in natural convection systems,
- Semi-active heat sinks which leverage off existing fans in the system,
- Active heat sinks employing designated fans for forced convection system,
- Liquid cooled cold plates employing tubes in block design or milled passages in brazed assemblies for the use of pumped water, oil or other liquids, and
- Phase change recirculating systems including two-phase systems that employ a set of boiler and condenser in a passive, self driven mechanism.

In this study, active heat sinks to cool central processing units (CPUs) of desktop computers are investigated.

1.1 System Constraints

During the design period of a heat sink the system constraints are to be determined first. System constraints are parameters that are out of control of the designer.

Heat to be removed: The most important system constraint is the rate of heat to be removed. It is generally assumed to be a fixed value, which is in fact the maximum heat dissipation rate of the electronic component even if the heat dissipation has a transient manner. The dissipated heat is due to the inefficiency of the electronic component and it is the difference between the input and output electrical power.

The maximum operating temperature: It is generally determined by the material properties of the electronic component. Most components which are not specifically designed for military applications have a maximum operating temperature which is less than 100 °C. Allowable thermal resistance is calculated

by using the dissipated power and the temperature difference between the maximum operating temperature and the ambient temperature. A computer using a CPU with 40 W heat dissipation rate and 80 °C of maximum operating temperature in an ambient of 30 °C, needs a heat sink with thermal resistance of 1.25 K/W or lower. This number should include the thermal resistance of the thermal interface material used to bond the heat source and heat sink and also chip's own internal thermal resistance from its junction to the chassis.

Ambient temperature: Since the air blown on the heat sink by the fan is at the temperature of the ambient, the thermal resistance is calculated by using the ambient temperature. For closed domains such as a computer chassis, the air inside the chassis will be hotter than the outside air, so average temperature of inside air instead of ambient air temperature must be used for thermal resistance calculations.

The maximum volume of the heat sink: This is another constraint when limited space around circuit boards is considered. For forced convection applications, the size of the fan should also be considered. A typical heat sink, Alpha PAL 8045A, occupies a total volume of 80x80x84 mm³, including the fan. For applications where the electronic box does not have enough space, heat pipes may be used to carry the heat load to a location where more space is available to use a big heat sink.

Altitude: Elevation of the electronic system to be cooled from sea level also plays a role in heat transfer due to the density variations of air. Since air is less dense at high altitudes than the sea level, its convective capability decreases. This means that higher cooling rates are needed as the altitude increases. These effects may be important for some applications such as aviation electronics. Chapman [4] shows how altitude changes affect the heat transfer. Also, Rhee and Azar propose a formula to extrapolate any temperature calculation at sea level to any altitude [5].

Sealing: In some cases the necessity for sealing out the dust and sand creates another system constraint. It prevents the use of external fans, as a result, cooling mechanisms are limited to radiation and natural convection through external surfaces [6]. If a fan is to be used, blowing fans are preferred since they increase the static pressure inside the chassis. Air filter is considered for sucking fans especially when the components are sensible to dust.

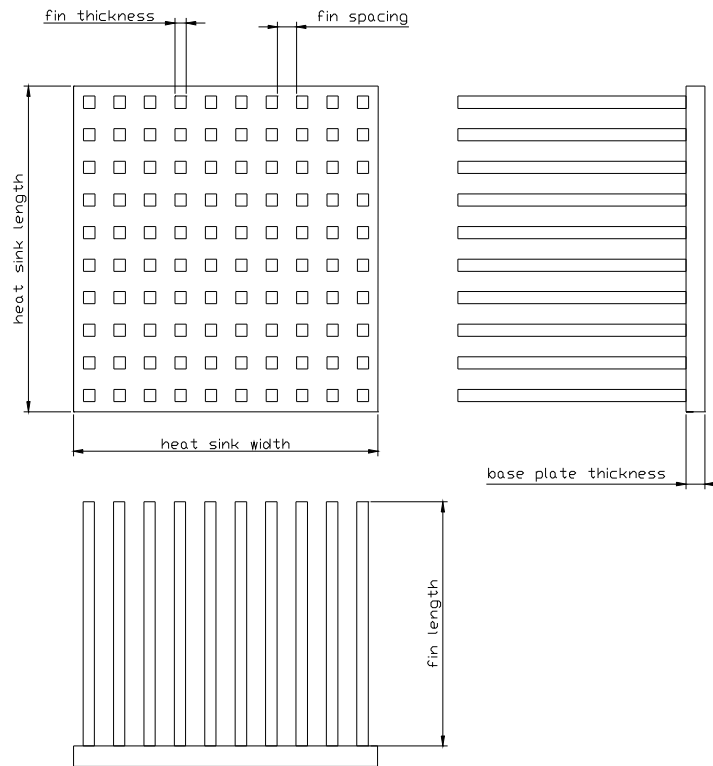


Figure 1.1 Heat sink design parameters

1.2 Design Parameters

Once the system constraints are determined, design parameters are to be considered. The design parameters include the heat sink material, the number and geometry of the fins and their alignment and the base plate thickness as

shown in Fig. 1.1. In order to obtain the minimum thermal resistance and pressure drop, each of these parameters must be designed well.

Materials: Heat sink materials are generally etched silicon for small dimensions and metals for larger sizes. Metals with high thermal conductivity and relatively low cost are preferred, like aluminum and copper. Combinations of different materials are possible like the use of aluminum fins bonded to a copper base as in Swiftech 462-A heat sink (Figure 1.2). Although the thermal conductivity of zinc is lower compared to that of aluminum and copper, it may also be a good material for electronic cooling purposes (Figure 1.3). When zinc added to an alloy, it eliminates porosity in the casting process, which is an advantage over aluminum and copper since they are not pore free after the casting.

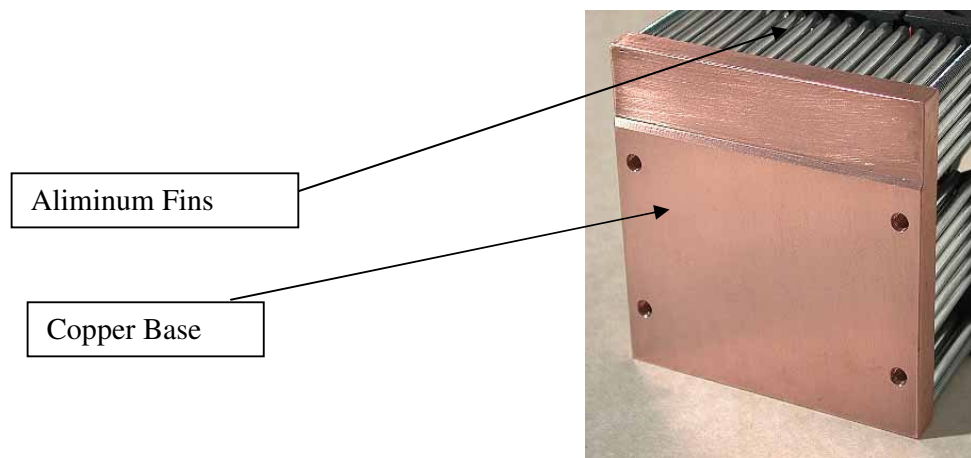


Figure 1.2 Bottom view of Swiftech 462-A. (Adapted from [7])

The number of the fins: It is one of the most important factors for heat sink performance. A heat sink designed for electronics cooling is a compact heat exchanger for which the ratio of heat transfer area to occupied volume is very large. The heat transfer area is enhanced by use of fins. Therefore increasing the number of fins provides more area for heat transfer. Increasing the number of fins from 238 to 294, Hedgehog increased the heat transfer area by 8.4 % and

approximately 10 % efficiency is assured in the succession of Hedgehog-238M to Hedgehog-294M [7]. However, it should be noted that increasing the number of fins creates an adverse effect, which is the increased static pressure drop. In order to overcome higher pressure drops, higher pumping powers are needed, which requires the installation of more powerful fans or blowers.

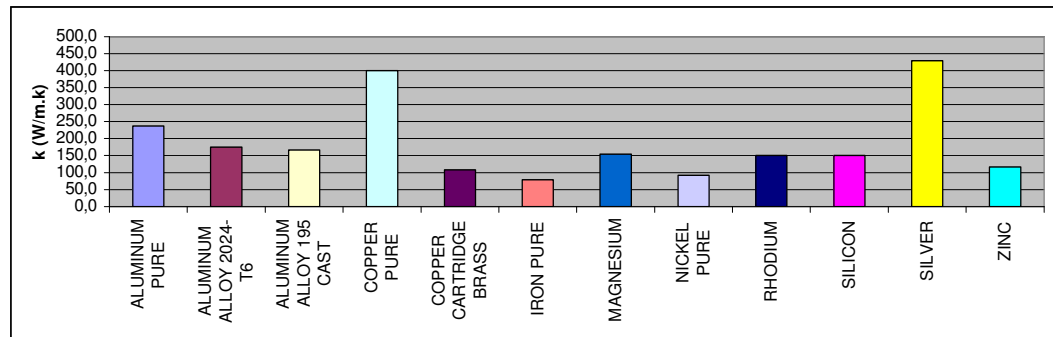


Figure 1.3. Thermal conductivities of common heat sink materials and possible candidates (adapted from [8])

Fin shapes: Different kinds of heat sink geometries are possible. Pin fins, straight fins, fluted fins, wavy fins and fins with non-standard geometry are possible. The most common ones are pin fins whose cross section can be round, square, elliptical, hexagonal or any other suitable geometry. A round cross section pin fin heat sink design is used in Global Win CDK38 (Fig 1.4). Straight fins that have rectangular cross sections are also widely used. Depending on the spacing among the fins of a heat sink, flow requirements and pressure drops may differ. Design engineers try to achieve the minimum thermal resistance with the pressure drop as low as possible by modifying the fin shapes. Extensive literature is available on this subject.

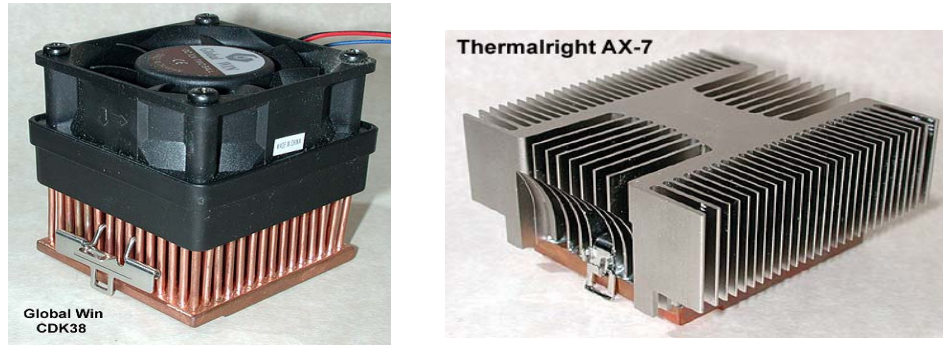


Figure 1.4. Two heat sinks with different fin geometry (adapted from [7])

Chapman *et al.* [9] showed that for the horizontal flow case using elliptical pin fins instead of rectangular ones reduces the vortex shedding and minimises the pressure drop. Consequently, the thermal resistance is reduced due to the lower temperatures which is a result of larger heat transfer area exposed to the flow.

Fluted and wavy heat sinks are not commonly used due to performance and manufacturability problems. Sikka *et al.* [10] showed such heat sinks did not yield significantly better thermal resistance than the conventional heat sinks for natural and low velocity forced convection.

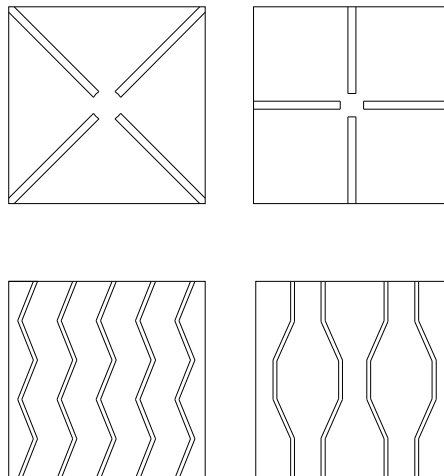


Figure 1.5. Examples of fluted heat sinks (at the top) and wavy heat sinks (at the bottom).

Sathyamurthy [11] demonstrated that when the fins of a rectangular cross section fin heat sink are divided into pieces in the flow direction and forming a staggered alignment, the thermal performance is enhanced by 8 % at the expense of 10 % to 20 % pressure drop. The reason is that a staggered fin heat sink enhances heat removal by repeated interruption and re-initiation of the boundary layer on the fin surfaces. Understanding this phenomenon, the design engineers prefer to install pin fin or divided fin heat sinks instead of planar fin heat sinks.

Fin alignment: Alignment of the fins on the base plate plays an important role especially for the heat sinks which are cooled by fans installed by their side. We only considered the heat sinks that are cooled by fans on the top. For side cooled heat sink, fin alignment may be inline or staggered. Although the staggered design is superior to the inline design under the same flow conditions, Dvinsky *et al.* [12] showed that inline design performs better than staggered for their specific case when the same fan is used. The explanation for this behaviour is the higher flow resistance of the staggered heat sink, which causes more air to bypass the heat sink.

Base plate thickness and fin height: These two parameters are to be handled together due to the frequently encountered space limitations. Base plate thickness accounts for the uniform distribution of heat through the base of heat sink, since electronic components are generally smaller than the heat sinks. Although base plates are generally square, they can also be rectangular, round or irregular in shape. If the base plate thickness increases then the fin length can be shorter. Technically, fins can be manufactured with a height approximately 80 times their thickness or diameter but since the rate of increased performance becomes less as height is increased, fin height of 45 times the thickness is the suggested maximum [13].

1.3 Other Parameters

If a fan is specified for a system, pressure drop, volumetric flow rate and flow cross sectional area also become system constraints. Otherwise they are the design parameters.

Pressure drop: Pressure drop is the resistance to the air movement and it is related with flow cross sectional area, fin spacing and fin length. The heat sink should be designed so as to yield a smaller pressure drop than the static pressure of the fan. The heat sink selected or designed changes the total pressure drop of the system, although it is not a very major difference, the operating point which is the intersection of the system impedance curve and the fan impedance curve may shift.

Volumetric flow rate: Volumetric flow rate is the velocity times the cross sectional area of the flow. Velocity magnitude of the incoming air is the dominant factor creating turbulence. Therefore if the fan is specified, the velocity of the air and the flow regime are known.

Flow inlet velocity as a design parameter is also surveyed in the literature. Increasing the flow inlet velocity thus the volumetric flow rate, which results in turbulence, the thermal resistance may be reduced by 35 % compared to the same geometry with laminar flow [14].

Flow cross sectional area: Flow cross sectional area is known as long as the fan dimensions are known. Designing a heat sink with a smaller cross sectional area than the flow area creates the by-pass of air. Since some of the air delivered by the fan will not participate in the heat transfer, efficiency is reduced. Ducting the coolant fluid to and from the heat sink through tubes, it is demonstrated that larger heat removal capabilities are achievable as the by-pass of air is prevented [15].

1.4 Fan Selection

For systems where forced convection is the main cooling mechanism, fan selection plays an important role. Fans utilise the motor torque to output a volumetric flow of air at a given pressure. Axial fans deliver air in the direction parallel to the fan blade axis. They can deliver high flow rates, but tend to work against low pressure [16]. If there is excessive pressure drop, blowers may be preferred. However, they deliver less air than axial fans and the air flow direction is perpendicular to the fan blade axis.

Fan selection is generally driven by system characteristics. Required airflow, system pressure drop, acoustics restrictions, reliability of the fan are the leading parameters affecting the fan selection.

Fan flow rate: The required volumetric flow rate, G , depends on dissipated heat (Q), temperature difference (ΔT) and the fluid properties; density (ρ) and specific heat (C_p).

$$Q = \dot{m} \cdot c_p \Delta T \quad (1.1)$$

$$\dot{m} = \rho G \quad (1.2)$$

$$G = \frac{Q}{\rho C_p \Delta T}$$

For an electronic component dissipating 80 W with the maximum operating temperature of 60 °C and the ambient temperature of 25 °C, the required volumetric flow rate is 10 cubic feet per minute (CFM) from the above equation. Nevertheless, installing a 10-CFM fan would be insufficient to remove the 80 watts. The geometry and the alignment of the fins determine how resistive they

are to the airflow. As a result of this resistance, flow bypasses the heat sink by a considerable amount. Therefore fans delivering air as much as 30-CFM may be necessary. Simons and Schmidt propose a simple method to estimate the flow by-pass [17]. They solve the Bernoulli equation and combine it with mass balance to find the velocity of by-pass air.

Fan stacking: It is essential to install multiple fans when airflow rate is not enough or a single fan cannot overcome the system pressure drop. Installing two or more fans side by side, i.e. in parallel, increases the volumetric flow rate. Stacking them one upon another, i.e. in series, enhances the static pressure.

Reliability: Fans are the least reliable parts of cooling systems. They have finite lifetimes like any other component with moving parts. The bearing used in the fan determines its reliability and cost. Sleeve bearing fans are the cheapest with 10000 hours of lifetime. Single ball single sleeve bearing fans carry a typical rating of 20000 hours. Dual ball bearing fans are the most reliable rated for 50000 hours with the highest price [18]. A suitable fan type should be selected according to the lifetime of the application. Single ball single sleeve bearing fans are generally enough for CPU cooling applications.

Noise levels: There are a few reasons of fan noise. Improper blade geometry is the main reason of noise. If the flow is not parallel to the fan blades from leading to the trailing edge and if separation from the blades occurs, then fan operates noisily. Another reason is the tip vortex generated between the fan tip and the casing. Gap between the fan and the casing is generally 3 % of the fan diameter, in order to decrease the noise, this gap is sometimes increased which results in the loss of performance. Vibration is also a reason of flow generated noise which should be avoided. Although there are many types of fans, tube axial fans are preferred for CPU cooling purposes. The main reason is that they are the quietest of all. The noise levels for today's coolers are between 35 to 70 dB [19]. The

experimental data of fan noise levels in Table 1.1 shows that the noise generation is mainly due to the fan selected. Fan1 is used to cool seven different heat sinks and noise levels are almost the same. Two different fans, fan2 and fan3 are installed over identical heat sinks and noise levels are different.

Table 1.1: Fan noise levels (Adapted from [19])

Heat Sink	Fan Type	Noise Generated
Thermalright SK6	1	61 dB
Kanie Hedgehog 294M	1	61 dB
Kanie Hedgehog	1	61 dB
Taisol CGK760xx2	1	61 dB
Glacialtech Igloo 2300	1	61 dB
Akasa Silver Mountain	1	62 dB
Zalman CNPS5000	1	62 dB
Zalman CNPS5000	2	52 dB
Zalman CNPS5000	3	58 dB

Fan specifications: A typical fan is identified by its numerical specifications. They describe the fan size, flow rate, rotation speed and power requirement. [20]

- Sizing numbers: They designate the dimensions of the fan. A 60x60x25 fan has the following dimensions; 60 mm length, 60 mm width, and 25 mm height.

- Fan flow rate: The most important feature of the fan is its flow rate. It is generally expressed as cubic feet per minute, CFM, which corresponds to 0.028317 cubic meters per minute.
- Rotation speed: Specifying the rotation speed of a fan is the most common way of designating it, e.g. Delta 7K rpm fan, which means the fan has a speed of 7000 rpm.
- Power requirement: Power used by a DC fan is the voltage across it multiplied by the current passing through.

Flow direction: After selecting the fan, the flow direction is determined. A blowing fan pushes air onto the heat sink whereas a sucking fan pulls air from the heat sink. When a fan sucks, the air at ambient temperature contacts the hottest part of the heat sink, which is the closer sections to the heat source, and air warms up quickly. This, results in lower efficiencies, therefore fans are generally installed to blow. Therefore, the air at ambient temperature can not heat up too much before it reaches down to the hottest parts of the heat sink.

1.5 Thermal Interface Materials

Once the heat sink and the fan, i.e., the cooling assembly is designed, a proper material should be selected to join the heat sink and the semiconductor, i.e. the heat source. There are various thermal interface materials serving for this purpose. Although they seem as additional thermal resistances to heat flow, they form thin layers with high thermal conductivities and minimise the contact discontinuities.

All solid surfaces no matter how smooth they are have certain roughness. Therefore when two surfaces come into physical contact, less than 1 % of the surfaces touch each other [21]. The remaining area is filled with air, which is a

poor medium for heat transfer. Therefore a more conductive material should replace air. Thermal greases, thermal compounds, elastomers or adhesive films may be used as thermal interface materials. Table 1.2 shows the thermal resistances of these materials when used to join a Pentium test chip and a Wakefield pin fin heat sink. Yovanovich *et al.* [22] present correlation equations to calculate interface resistances for conforming rough surfaces.

Table 1.2 Thermal resistances of dry joint and thermal interface materials.
(Adapted from [21])

Interface	Thermal conductivity (W/m.K)	Thermal resistance (K/W)
Dry joint	N/A	2.9
Thermal grease	0.7	0.9
Thermal compound	1.2	0.8
Elastomer	5.0	1.8
Adhesive Film	0.7	2.7

Although thermal grease and thermal compound have very improved thermal resistances, the other two may also be preferred. Elastomers are typically used for devices where electrical isolation is required. The advantage of adhesive films is that they do not require any mechanical support like spring clips to attach heat sink to the CPU.

1.6 Assumptions

In order to simplify the problem, compressibility effects and radiation heat transfer can be neglected for heat transfer at forced convection cooled heat sinks.

Detailed information regarding the compressibility and radiation is given in Chapter 2, section 2.2.3. Some geometrical details are ignored for further simplifications.

The very detailed geometries, which are not directly affecting the solution are approximated by lumped parameter models. Solving fans with rotating reference frames or sliding mesh approaches brings too much computational effort. Therefore fans are also modelled as lumped parameter models. Lumped parameter modelling means that modelling the object with approximations, without using the exact geometry. For fans, the fan is modelled as a surface which creates a pressure difference across that face. The blades of the fan are not modelled as shown in Figure 1.6. The advantage of this type of modelling is that it saves a lot of time and computational power but the drawback is the swirl which can not be modelled with lumped parameter modelling.

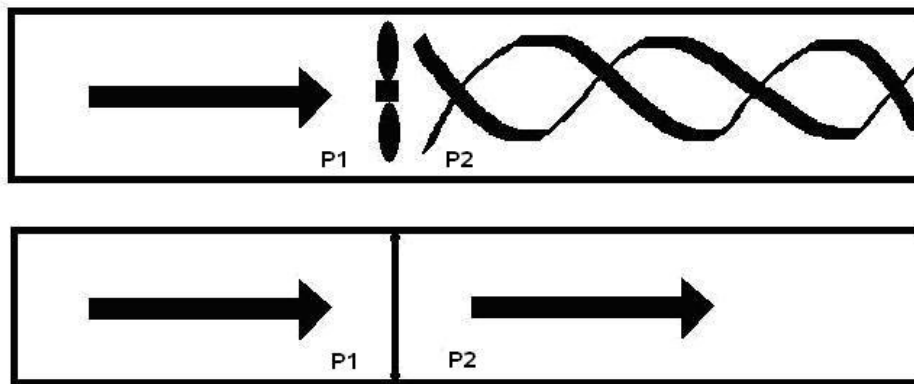


Figure 1.6 Exact modelling of the fans at the top and lumped parameter modelling at the bottom

Steinberg [1] proposes that the position of fan blades within an axial flow fan housing can be a critical factor in determining how well the fan will perform especially for fans having rotational speeds more than 8000 rpm, which is not the

case for CPU cooling applications. Other than fans, grilles and power supply are too complicated to be modelled exactly. Therefore, lumped models are used for them also.

1.7 Solution Approaches

After determining the system constraints and the design parameters, now we concentrate on solving the conjugate heat transfer, i.e. simultaneous conduction and convection, problem. Various methods are available for the solution.

Moffat [23] claims that the flow and heat transfer situations encountered in electronics cooling applications are much more challenging than those in heat exchangers and as complex as those encountered in gas turbine blade cooling. Since it is almost impossible to get a detailed solution of the thermal and flow fields in a complicated electronic box, like a computer chassis, new areas are emerging for thermal design of such systems. Although known for years, Computational Fluid Dynamics simulations have not entered electronics cooling area for a long time. Before the last decade, it was very expensive to perform CFD calculations, but with the introduction of high power workstations and personal computers, the cost of such computations has been drastically reduced [24].

Several researchers have worked on conjugate heat transfer at electronic systems via CFD. Yu and Webb [25] simulated a complete desktop computer system which uses an 80 W CPU. With the addition of other components (memory, chipset, AGP, PCI cards, floppy drives) a total of 313 W heat is dissipated into the system. They solved the whole domain with a commercially available software, Icepak. To decrease the complexity of their model they modelled CPU heat sink as a volume resistance having the same impedance with the detailed geometry. They improve the cooling of PCI cards with PCI side vents and baffle.

Biswas *et al.* [26] also used Icepak to study the airflow in a compact electronic enclosure. Their aim was to investigate the pressure loss due to the presence of the inlet and outlet grilles. They consider to the use of fan curves obtained from the manufacturer since the fan curve may need to be modified if the fan is not closely ducted.

Argento, Joshi and Osterman [27] have studied system level electronic packaging thermal design not only computationally but also verifying it experimentally. After the verification they worked on redesign of an inlet plenum. Their implemented modification resulted in 56 % reduction of the surface temperature.

Some relatively older studies use CFD for heat sink simulations only. Linton and Agonafer [28] compare the results of detailed CFD modelling of a heat sink with experimental data. Then they present a technique for representing the heat sink in a coarse manner for less time consuming simulations. Their coarse model agrees well with the detailed model without losing the characteristics of the heat sink.

Sathyamurthy and Runstadler [29] studied planar and staggered heat sink performance with a commercially available software, FLUENT. Their computational results agreed well with the experimental ones. They found that the thermal performance of staggered fin configuration is superior over planar fin configuration. However the pressure drop requirements for the staggered fin heat sink was greater than those for the planar case.

Eveloy *et al.* [30] used Flotherm software to provide a perspective on the current capabilities of CFD as a design tool to predict component temperature on printed circuit boards. Their computations predict the component operating temperature in an accuracy range of 3 °C to 22 °C, with up to 35 % error. They suggest that component junction temperature would need to be experimentally measured when used for strategic product design decisions. They think that the source of

error is due to the turbulence models employed. They suggest using flow visualization in the early design phase to identify aerodynamically sensitive regions on the board, where temperature distributions should be handled with care.

This study makes use of CFD for the conjugate heat transfer simulations in a whole computer chassis. Icepak and FLUENT are used simultaneously for the CFD calculations.

CHAPTER 2

CFD MODELS and EQUATIONS SOLVED

In CFD calculations, there are three main steps.

- 1) Pre-Processing
- 2) Solver Execution
- 3) Post-Processing

Pre-Processing is the step where the modeling goals are determined and computational grid is created. In the second step numerical models and boundary conditions are set to start up the solver. Solver runs until the convergence is reached. When solver is terminated, the results are examined which is the post-processing part.

2.1 Pre-Processing

In this study, the aim is to investigate the cooling characteristics of different heat sinks designed to cool the central processing unit (CPU) of a computer. So, an adequate numerical model is to be created. Pre-processing is the most time consuming and least knowledge requiring part. There are two important points here. The first one is the size of the domain, and the second one is the density and quality of the computational grid.

Model size is the computational domain where the solution is done. It is important to build it as small as possible to prevent the model to be computationally expensive. On the other hand it should be large enough to resolve all the fluid and energy flow affecting the heat transfer around the CPU. In our problem, domain is selected to be the whole computer chassis. Although the flow outside the chassis, namely natural convection affects the heat transfer inside the chassis, lumped parameter model approaches will be used to account

for the flow outside the chassis. Inside the chassis, CPU, CPU cooler, power supply, floppy and hard drives, mainboard and other cards are modeled. Since there were no CAD data for the chosen problem geometry, all the devices inside the case are created using Icepak's object based geometry creation tools. Small details which are considered not to be affecting the solution, like wires, cables and electronic components such as transistors, capacitors etc. are not modeled. To make the models computationally inexpensive such that the computer resources available can solve, the fans, the grilles and the power supply are modeled as lumped parameter models. Details of the computational model are given in Appendix A.

A high quality unstructured hexahedral mesh is generated before the solution of the governing equations. Mesh is non-conformal in order to decrease the total number of cells in the computational domain. Mesh generation algorithms and quality aspects are explained in Appendix B.

2.2 Solver Execution

2.2.1 Governing Equations of Fluid Flow

The most general form of fluid flow and heat transfer equations of compressible Newtonian fluid with time dependency is given as follows:

$$\text{mass:} \quad \frac{\partial \rho}{\partial t} + \nabla \cdot (\rho \vec{V}) = 0 \quad (2.1)$$

$$\text{x-momentum:} \quad \frac{\partial(\rho u)}{\partial t} + \nabla \cdot (\rho u \vec{V}) = -\frac{\partial p}{\partial x} + \frac{\partial \tau_{xx}}{\partial x} + \frac{\partial \tau_{yx}}{\partial y} + \frac{\partial \tau_{zx}}{\partial z} + S_{Mx} \quad (2.2)$$

$$\text{y-momentum:} \quad \frac{\partial(\rho v)}{\partial t} + \nabla \cdot (\rho v \vec{V}) = -\frac{\partial p}{\partial y} + \frac{\partial \tau_{xy}}{\partial x} + \frac{\partial \tau_{yy}}{\partial y} + \frac{\partial \tau_{zy}}{\partial z} + S_{My} \quad (2.3)$$

$$\text{z-momentum:} \quad \frac{\partial(\rho w)}{\partial t} + \nabla \cdot (\rho w \vec{V}) = -\frac{\partial p}{\partial z} + \frac{\partial \tau_{xz}}{\partial x} + \frac{\partial \tau_{yz}}{\partial y} + \frac{\partial \tau_{zz}}{\partial z} + S_{Mz} \quad (2.4)$$

energy:
$$\frac{\partial(\rho h_0)}{\partial t} + \nabla \cdot (\rho h_0 \vec{V}) = -p \nabla \cdot \vec{V} + \nabla \cdot (k \nabla T) + \Phi + S_h \quad (2.5)$$

equation of state:
$$p = \rho RT \quad (2.6)$$

where ρ is the density, u, v and w are velocity components, \vec{V} is the velocity vector, p is the pressure, S terms are the source terms and τ terms are the viscous stress components which are defined for a Newtonian fluid as.

$$\tau_{xx} = \lambda \left(\frac{\partial u}{\partial x} + \frac{\partial v}{\partial y} + \frac{\partial w}{\partial z} \right) + 2\mu \frac{\partial u}{\partial x} \quad (2.8)$$

$$\tau_{yy} = \lambda \left(\frac{\partial u}{\partial x} + \frac{\partial v}{\partial y} + \frac{\partial w}{\partial z} \right) + 2\mu \frac{\partial v}{\partial y} \quad (2.9)$$

$$\tau_{zz} = \lambda \left(\frac{\partial u}{\partial x} + \frac{\partial v}{\partial y} + \frac{\partial w}{\partial z} \right) + 2\mu \frac{\partial w}{\partial z} \quad (2.10)$$

$$\tau_{xy} = \tau_{yx} = \mu \left(\frac{\partial u}{\partial y} + \frac{\partial v}{\partial x} \right) \quad (2.11)$$

$$\tau_{xz} = \tau_{zx} = \mu \left(\frac{\partial u}{\partial z} + \frac{\partial w}{\partial x} \right) \quad (2.12)$$

$$\tau_{yz} = \tau_{zy} = \mu \left(\frac{\partial v}{\partial z} + \frac{\partial w}{\partial y} \right) \quad (2.13)$$

Here, μ is the dynamic viscosity. λ is the second viscosity and a good approximation for gases is taking $\lambda = -\frac{2}{3}\mu$.

In Eq.2.5, Φ is the viscous dissipation term. It is always positive and represents the dissipation of mechanical energy into heat. This dissipation term is usually very small except for high Mach number flows.

$$\Phi = \lambda (\nabla \cdot \vec{V})^2 + \mu \left[2 \left(\frac{\partial u}{\partial x} \right)^2 + 2 \left(\frac{\partial v}{\partial y} \right)^2 + 2 \left(\frac{\partial w}{\partial z} \right)^2 + \left(\frac{\partial u}{\partial y} + \frac{\partial v}{\partial x} \right)^2 + \left(\frac{\partial u}{\partial z} + \frac{\partial w}{\partial x} \right)^2 + \left(\frac{\partial v}{\partial z} + \frac{\partial w}{\partial y} \right)^2 \right] \quad (2.14)$$

h_0 is the total enthalpy, which is defined as

$$h_0 = h_e + \frac{1}{2}(u^2 + v^2 + w^2) = i + p/\rho + \frac{1}{2}(u^2 + v^2 + w^2) = E + p/\rho \quad (2.15)$$

where h_e is the enthalpy defined as $h_e = \int_{T_{ref}}^T C_p dT$, i is the internal thermal energy, E is the total energy of the fluid which is the sum of internal thermal energy and kinetic energy.

2.2.2 Mathematical Model

Computer chassis is the computational domain. Figure 2.1 shows the components of the chassis. It is a 3D chassis. CPU, CPU heat sink, CPU fan, AGP, AGP heat sink, AGP fan, chipset, chipset heat sink, mainboard, memory cards, miscellaneous cards, DVD-Rom, CD-Rom, hard disk drive, floppy drive, power supply, system fans and chassis grilles are shown on the figure. The geometric details are dense around the CPU heat sink so a closer view is shown in Figure 2.2. Since the scope of this study is investigation of temperature distributions on CPU heat sinks, closer view of one of the CPU heat sinks that is investigated in this study is also given in Figure 2.3.

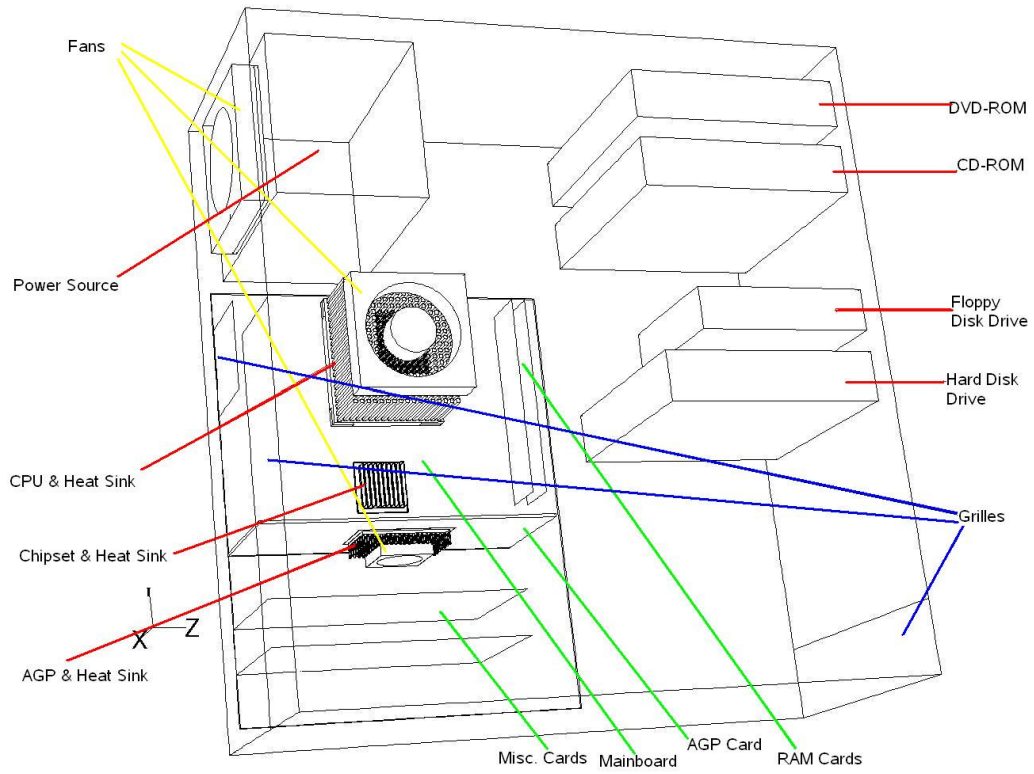


Figure 2.1 Computational domain

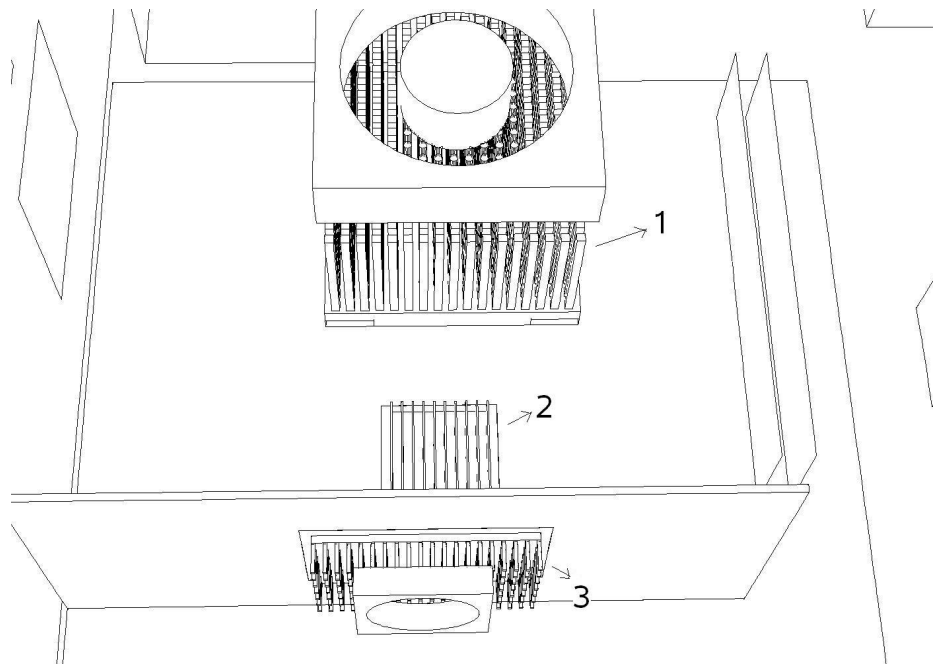


Figure 2.2 CPU Heat sink (1), Chipset heat sink (2) and AGP heat sink (3)

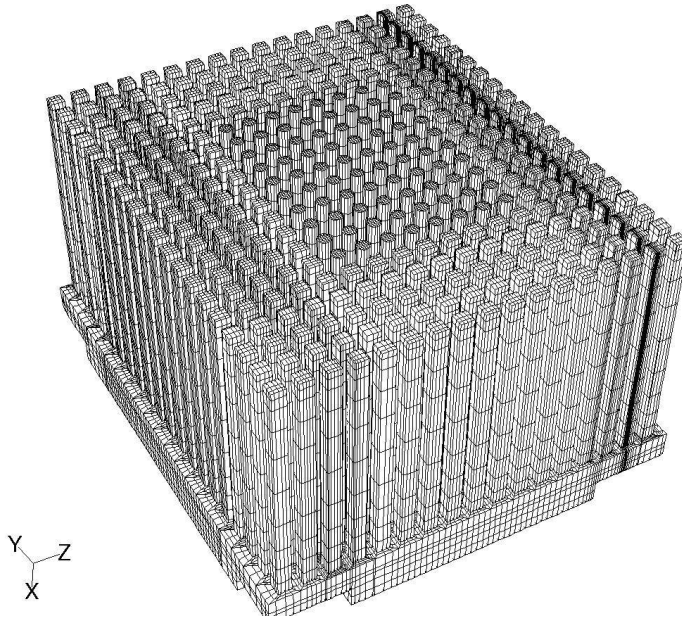


Figure 2.3 Alpha CPU heat sink

2.2.3 Flow Configuration and Boundary Conditions

The compressibility effects and turbulence inside the chassis are the parameters changing the governing equations to be solved. Their roles in this study are explained as well as radiation, interior and boundary conditions.

Compressibility:

The fluid in the domain is air. The compressibility effects are ignored due to the low speeds. For a 60 mm diameter fan with 60 CFM of air flow, velocity of the incoming air and Mach number are calculated as:

$$V_a = \frac{G}{\pi \cdot r^2} \quad (2.16)$$

$$Ma = \frac{V_a}{c} \quad (2.17)$$

$$V_a = 2.504 \text{ m/s}$$

$$Ma = 7.364 \times 10^{-3}$$

Here, V_a is the velocity of air, G is the fan flow rate, r is the fan diameter, c is the speed of sound which is taken as 300 m/s and Ma is the Mach number. Although air is a compressible fluid, incompressible flow assumption is valid as long as the Mach number is smaller than 0.3 [36]. The fans that will be used in this study deliver less air than 60 CFM and Mach number is much less than 0.3; therefore incompressible flow assumption will be used in this study.

Turbulence:

The flow inside the chassis is turbulent regardless the Reynolds number. The existence of several different components and several heat sources together with the vortices created by the fans make the flow regime turbulent inside the chassis. Details of turbulence and its modelling are given in Appendix D.

Radiation:

Radiation is one of the important things to be considered when flow inside a computer chassis is to be solved. However it is necessary to take it into account when the flow is not forced by fans. For a chassis inside which natural convection is the dominant heat transfer mode, radiation should be taken into account. In our case, the main heat transfer mode is forced convection.

The contribution of radiative heat transfer can be roughly estimated by calculating radiative heat transfer rate for a heat sink operating to cool an electronic component whose maximum operating temperature must be 60 °C.

Since, only the radiative heat transfer between the imaginary surface bounding the heat sink and the surroundings is important, the heat sink is taken as a box with dimensions 80x80x60 mm³. The heat sink dissipates 70 W of heat. It is assumed that the heat sink temperature is uniform and 55 °C and the surroundings temperature is 35 °C. The following results showed that even with a view factor of 1 and surface emissivity of 0.97 (Table D.1), the net radiative heat transfer accounted for is about 5 % of the total heat transfer.

$$T_h = 55 + 273 = 328 \text{ K}$$

$$T_{surr} = 35 + 273 = 308 \text{ K}$$

$$\sigma = 5.67 \times 10^{-8} \text{ W/m}^2 \cdot \text{K}^4$$

$$A = 0.08 \times 0.08 + 4 \times 0.06 \times 0.08 = 0.026 \text{ m}^2$$

$$\varepsilon = 0.97$$

$$F = 1$$

$$Q = \varepsilon \sigma F A (T_h^4 - T_a^4) \tag{2.18}$$

$$Q = 3.68 \text{ W}$$

Here, T_h is the temperature on the fin surfaces, T_{surr} is the temperature of the surroundings, σ is the Stefan-Boltzmann constant, A is the heat transfer area calculated for the outward looking sides of the imaginary box, ε is the surface emissivity, F is the view factor and Q is the radiative heat transfer rate.

When the radiation among the fins themselves is ignored, the radiation heat transfer is calculated as 3.68 W which is negligible. Yet, two analyses comparing the effects of radiation heat transfer can be found in Chapter 3. Details of radiation modelling are given in Appendix D.

Boundary Conditions:

Since Navier-Stokes equations are solved inside the domain, no-slip boundary condition is applied to all walls in the domain. Therefore, at all surfaces

$$u = v = w = 0 \quad (2.19)$$

It is assumed that system fan does not drive a flow cell around the computer chassis and the heat transfer mechanism at the chassis outer walls is natural convection. Heat transfer coefficients at the outer walls are estimated from the correlations. In order to use the correlations, the average wall temperature must be prescribed. To do that, a first cut analysis must be run. As the typical values of the natural convection heat transfer coefficient lies between 2 and 25 W/m²K, a value of 5 W/m²K is selected to be the heat transfer coefficient at the computer chassis walls. The analysis results by taking ambient temperature as 30 °C gives an average wall temperature of 36°C at the walls and then heat transfer coefficients are calculated using this value and the available correlations. [8]

$$Ra_L = Gr_L Pr = \frac{g\beta(T_s - T_\infty)L^3}{\nu\alpha} \quad (2.20)$$

Where surface temperature $T_s = 36^\circ\text{C}$, free stream temperature $T_\infty = 30^\circ\text{C}$, length of the vertical plate $L = 0.444$ m, gravity g is 9.81 m/s², kinematic viscosity $\nu = 15.89 \times 10^{-6}$ m²/s and thermal diffusivity $\alpha = 22.50 \times 10^{-6}$ m²/s for 300 K.

$$Ra_L = \frac{9.81 \frac{1}{303} (36 - 30)(0.444)^3}{15.89 \times 10^{-6} \cdot 22.50 \times 10^{-6}} = 4.8 \times 10^7$$

Since Ra is less than 1×10^9 , the flow is laminar. Using correlations for laminar natural convection on the vertical plate;

$$\overline{Nu}_L = 0.68 + \frac{0.670 Ra_L^{1/4}}{[1 + (0.492 / Pr)^{4/16}]^{4/9}} \quad (2.21)$$

$$\overline{Nu}_L = 0.68 + \frac{0.670 Ra_L^{1/4}}{[1 + (0.492 / 0.7)^{4/16}]^{4/9}} = 42.4$$

$$h = \frac{\overline{Nu}_L k}{L} \quad (2.22)$$

Where thermal conductivity of air $k=27 \times 10^{-3}$ W/mK

$$h \approx 3 \text{ W/m}^2\text{K}$$

Second analysis is done by applying this value as the computer chassis wall heat transfer coefficients and it was seen that the average wall temperatures were very close to 36°C, therefore there is no need to continue with the iterations.

Similarly, for the horizontal top plate Rayleigh number is calculated from 2.20. This time L , characteristic length, is calculated from $L=A/P$, where A is the plate surface area and P is the plate perimeter.

$$L = \frac{0.187 \times 0.424}{2(0.187 + 0.424)} = 0.065$$

$$Ra_L = \frac{9.81 \frac{1}{303} (36 - 30)(0.065)^3}{15.89 \times 10^{-6} \cdot 22.50 \times 10^{-6}} = 1.5 \times 10^5$$

Nusselt number for the corresponding Rayleigh number is defined as;

$$\overline{Nu}_L = 0.54 Ra_L^{1/4} \quad (2.23)$$

$$\overline{Nu}_L = 0.54 (1.5 \times 10^5)^{1/4} = 0.135$$

$$h = \frac{0.135 \times 27 \times 10^{-3}}{0.065} = 0.05 \text{ W/m}^2\text{K}$$

The calculated heat transfer coefficients are applied to all exterior walls of the chassis except the bottom horizontal wall which sits on the ground.

Interior Conditions:

The thermal boundary conditions for the objects inside the chassis are listed in table 2.1. A total of 252 W is dissipated.

Table 2.1 Interior conditions

Object Name	Material	Heat Dissipation Rates (W)
CPU	Silicon	70
AGP	Silicon	25
CD	Al	10
DVD	Al	10
Hard drive	Al	20
Floppy	Al	-
Chipset	Silicon	10
CPU heat sink	Al-Cu	-
AGP heat sink	Al	-
Chipset heat sink	Al	-
Power supply	Porous	75
Memory cards	FR4	6x2
Misc. cards	FR4	10x2
Mainboard	FR4	-

The fans inside the domain are modeled as circular surfaces which add momentum source to the flow. The added momentum source is given as the pressure rise across the fan versus the flow rate curve. From the system pressure curve, the point where the fan is going to operate is calculated iteratively. The relationship between the pressure and the flow rate is taken linearly.

Table 2.2 Fan conditions

Name of the fan	Pressure Rise	Max Flow rate
CPU Heat sink fan	25 Pa	30 cfm
Case fan	40 Pa	40 cfm
AGP Heat sink fan	25 Pa	25 cfm

The boundary condition for the power supply is different. The power supply is geometrically very complicated. Therefore it is modeled by simplifications. The power supply is a rectangular box which is a resistance to flow. The resistance is different in y-direction. The reason for this is to allow air to pass through the power supply more easily in y-direction than the other directions. This is accomplished by modeling the power supply as porous medium. The Porous medium modeling adds a momentum sink to the momentum equation which creates a pressure drop proportional to the velocity. The momentum sink is composed of two parts, the first term on the right hand side is the viscous loss term and the second term is the inertial loss term.

$$S_i = -\left(\frac{\mu}{\alpha}v_i + C_2 \frac{1}{2} \rho v_{mag} v_i\right) \quad (2.24)$$

Here α is the permeability, v_{mag} is the velocity magnitude. When it is defined separately in different directions, anisotropic permeability is modeled. C_2 is the inertial resistance factor which is 0 in our case due to the laminar flow assumption in the porous zone. In this case, Equation 2.24 simplifies to be the Darcy's law. [36]

2.2.4 Governing Equations to be Solved

Time independent flow equations with turbulence are to be solved. The viscous dissipation term will be omitted. Therefore the governing equations for the fluid flow, Equations 2.1-2.6 are modified as follows:

$$\text{mass:} \quad \nabla \cdot (\rho \vec{V}) = 0 \quad (2.25)$$

$$\text{x-momentum:} \quad \nabla \cdot (\rho u \vec{V}) = -\frac{\partial p}{\partial x} + \frac{\partial \tau_{xx}}{\partial x} + \frac{\partial \tau_{yx}}{\partial y} + \frac{\partial \tau_{zx}}{\partial z} + S_{Mx} \quad (2.26)$$

$$\text{y-momentum:} \quad \nabla \cdot (\rho v \vec{V}) = -\frac{\partial p}{\partial y} + \frac{\partial \tau_{xy}}{\partial x} + \frac{\partial \tau_{yy}}{\partial y} + \frac{\partial \tau_{zy}}{\partial z} + S_{My} \quad (2.27)$$

$$\text{z-momentum:} \quad \nabla \cdot (\rho w \vec{V}) = -\frac{\partial p}{\partial z} + \frac{\partial \tau_{xz}}{\partial x} + \frac{\partial \tau_{yz}}{\partial y} + \frac{\partial \tau_{zz}}{\partial z} + S_{Mz} \quad (2.28)$$

$$\text{energy:} \quad \nabla \cdot (\rho h_0 \vec{V}) = -p \nabla \cdot \vec{V} + \nabla \cdot (k_{eff} \nabla T) + S_h \quad (2.29)$$

$$\text{equation of state:} \quad p = \rho RT \quad (2.30)$$

In the energy equation effective thermal conductivity is defined as

$$k_{eff} = k + k_t \quad (2.31)$$

To handle turbulence, Reynolds averaging technique is employed. In Reynolds averaging, the solution variables are decomposed into mean and fluctuating components. For the velocity components,

$$u = \bar{u} + u' \quad (2.32)$$

where \bar{u} and u' are the mean and fluctuating velocity components for x-direction. Likewise, for pressure and other scalar quantities:

$$\phi = \bar{\phi} + \phi' \quad (2.33)$$

where ϕ is a scalar such as pressure or energy.

Before this form of equations is substituted into the instantaneous continuity and momentum equations, equations 2.24-2.26 are rewritten in a more compact form;

$$\text{x-momentum:} \quad \nabla \cdot (\rho u \vec{V}) = -\frac{\partial p}{\partial x} + \nabla \cdot (\mu_{eff} \nabla u) + S_{Mx} \quad (2.34)$$

$$\text{y-momentum:} \quad \nabla \cdot (\rho v \vec{V}) = -\frac{\partial p}{\partial y} + \nabla \cdot (\mu_{eff} \nabla v) + S_{My} \quad (2.35)$$

$$\text{z-momentum:} \quad \nabla \cdot (\rho w \vec{V}) = -\frac{\partial p}{\partial z} + \nabla \cdot (\mu_{eff} \nabla w) + S_{Mz} \quad (2.36)$$

where, effective viscosity is the sum of laminar viscosity μ and turbulent viscosity μ_t defined as;

$$\mu_{eff} = \mu + \mu_t \quad (2.37)$$

Now taking a time average, time (or ensemble) averaged Navier-Stokes equations are obtained. The bar over the mean velocity is dropped for convenience.

$$\text{x-momentum:} \quad \nabla \cdot (\rho u \vec{V}) = -\frac{\partial p}{\partial x} + \nabla \cdot (\mu_{eff} \nabla u) + \left[\frac{\partial (\rho \overline{u'^2})}{\partial x} - \frac{\partial (\rho \overline{u'v'})}{\partial y} - \frac{\partial (\rho \overline{u'w'})}{\partial z} \right] - S_{Mx} \quad (2.38)$$

$$\text{y-momentum:} \quad \nabla \cdot (\rho v \vec{V}) = -\frac{\partial p}{\partial y} + \nabla \cdot (\mu_{eff} \nabla v) + \left[\frac{\partial (\rho \overline{u'v'})}{\partial x} - \frac{\partial (\rho \overline{v'^2})}{\partial y} - \frac{\partial (\rho \overline{v'w'})}{\partial z} \right] - S_{My} \quad (2.39)$$

$$\nabla \cdot (\rho w \vec{V}) = -\frac{\partial p}{\partial z} + \nabla \cdot (\mu_{eff} \nabla w) +$$

z-momentum:
$$\left[-\frac{\partial(\rho \overline{u'w'})}{\partial x} - \frac{\partial(\rho \overline{v'w'})}{\partial y} - \frac{\partial(\rho \overline{w'^2})}{\partial z} \right] - S_{My} \quad (2.40)$$

Equations 2.40-2.40 are called Reynolds Averaged Navier-Stokes (RANS) equations. They have the same general form as the instantaneous Navier-Stokes equations, with the velocities and other solution variables now representing ensemble-averaged (or time-averaged) values. Additional terms now appear and they represent the effects of turbulence. The Reynolds stresses, numerator terms in the brackets, must be modeled in order to close the equation set. A common and relatively easy way to model these stresses is the Boussinesq approach which relates the Reynolds stresses to mean velocity gradients.

In order to simplify the notation, suffix notation will be used to define the Reynolds stresses. The convention of this notation is that i or $j=1$ corresponds to x-direction, i or $j=2$ corresponds to y-direction and i or $j=3$ corresponds to z-direction [33].

$$\tau_{ij} = -\overline{\rho u'_i u'_j} = \mu_{eff} \left(\frac{\partial u_i}{\partial x_j} + \frac{\partial u_j}{\partial x_i} \right) \quad (2.41)$$

Where the turbulence part, μ_t , of the effective viscosity has different definitions according to the turbulence model employed. In this study, the results were applied for two different approaches; zero-equation mixing length and κ - ϵ models. For zero-equation mixing length turbulence model,

$$\mu_t = \rho C_\mu l^2 \left| \frac{\partial u}{\partial y} \right| \quad (2.42)$$

Here C_μ is a constant and l is the length scale. For zero-equation models, no extra equation is solved for closure. However for κ - ε models, turbulence viscosity is defined as;

$$\mu_t = \rho C_\mu \frac{\kappa^2}{\varepsilon} \quad (2.43)$$

where $C_\mu = 0.0845$ which is a constant calculated using RNG theory. κ is the turbulence kinetic energy and ε is the turbulence dissipation rate. κ and ε are calculated by the following equations.

$$\nabla \cdot (\rho k \vec{V}) = \nabla \cdot (\alpha_\kappa \mu_{eff} \nabla \kappa) + G_\kappa + G_b - \rho \varepsilon - Y_M \quad (2.44)$$

$$\nabla \cdot (\rho \varepsilon u_i) = \nabla \cdot (\alpha_\varepsilon \mu_{eff} \nabla \varepsilon) + C_{1\varepsilon} \frac{\varepsilon}{\kappa} (G_\kappa + C_{3\varepsilon} G_b) - C_{2\varepsilon} \rho \frac{\varepsilon^2}{\kappa} - R_\varepsilon \quad (2.45)$$

α_κ and α_ε are inverse effective Prandtl numbers, $C_{1\varepsilon}$ and $C_{2\varepsilon}$ are model constants, G_κ represents generation of turbulence kinetic energy due to mean velocity gradients, G_b is the generation of turbulence kinetic energy due to buoyancy, Y_M is the contribution of the fluctuating dilatation in compressible turbulence to the overall dissipation rate. In our cases G_b and Y_M are zero.

2.2.5 Parameters and Unknowns

The reduced Navier-Stokes equations that FLUENT solves by using Finite Volume Method is given once more.

$$\nabla \cdot (\rho \vec{V}) = 0$$

$$\nabla \cdot (\rho u \vec{V}) = -\frac{\partial p}{\partial x} + \nabla \cdot (\mu_{eff} \nabla u) + \left[-\frac{\partial(\overline{\rho u'^2})}{\partial x} - \frac{\partial(\overline{\rho u'v'})}{\partial y} - \frac{\partial(\overline{\rho u'w'})}{\partial z} \right] - S_{Mx}$$

$$\nabla \cdot (\rho v \vec{V}) = -\frac{\partial p}{\partial y} + \nabla \cdot (\mu_{eff} \nabla v) + \left[-\frac{\partial(\rho \overline{u'v'})}{\partial x} - \frac{\partial(\rho \overline{v'^2})}{\partial y} - \frac{\partial(\rho \overline{v'w'})}{\partial z} \right] - S_{My}$$

$$\nabla \cdot (\rho w \vec{V}) = -\frac{\partial p}{\partial z} + \nabla \cdot (\mu_{eff} \nabla w) + \left[-\frac{\partial(\rho \overline{u'w'})}{\partial x} - \frac{\partial(\rho \overline{v'w'})}{\partial y} - \frac{\partial(\rho \overline{w'^2})}{\partial z} \right] - S_{My}$$

$$\nabla \cdot (\rho h_0 \vec{V}) = -p \nabla \cdot \vec{V} + \nabla \cdot (k_{eff} \nabla T) + S_h$$

$$p = \rho RT$$

Regarding these equations, the six unknowns are ρ , u , v , w , p and T . μ_{eff} and k_{eff} are defined as the sum of laminar and turbulent viscosity and thermal conductivity respectively as given in equations 2.31 and 2.37. Their solution depends on the turbulence model employed and for κ - ϵ models, two additional equations are also solved which are;

$$\nabla \cdot (\rho k \vec{V}) = \nabla \cdot (\alpha_\kappa \mu_{eff} \nabla \kappa) + G_\kappa - \rho \epsilon$$

$$\nabla \cdot (\rho \epsilon \vec{V}) = \nabla \cdot (\alpha_\epsilon \mu_{eff} \nabla \epsilon) + C_{1\epsilon} \frac{\epsilon}{\kappa} (G_\kappa + C_{3\epsilon} G_b) - C_{2\epsilon} \rho \frac{\epsilon^2}{\kappa} - R_\epsilon$$

For the above equations constants are as follows:

$$C_p = 1005 \text{ J/kgK}$$

$$k = 0.0261 \text{ W/mK}$$

$$\mu = 1.84 \times 10^{-5} \text{ kg/ms}$$

$$T_{ref} = 293.15 \text{ K}$$

$$C_\mu = 0.0845$$

$$C_{1\epsilon} = 1.42$$

$$C_{2\epsilon} = 1.68$$

$$\alpha_\kappa = 1.393$$

$$\alpha_\epsilon = 1.393$$

The details of how FLUENT solver works to solve the presented equations by means of pressure-velocity coupling, discretization and linearization are given in Appendix C.

CHAPTER 3

RESULTS OF CFD ANALYSES

3.1 Sources of Errors in CFD Calculations

There is always error in a CFD analysis. It is important to know the sources of these errors and take precautions accordingly.

The major source of error for a CFD analysis is due to the selected numerical method to solve Navier-Stokes equations. Some of the numerical techniques employed in CFD are Finite Difference Methods, Finite Element Methods and Finite Volume Methods. The one FLUENT uses is the Finite Volume Method and the source of error here arises when discretizing the transport equations. Interpolations are made to find values at the cell faces, whereas all the information is stored at the cell centers. This is the main approximation of the Finite Volume Method.

Second type of error is at the Boundary Condition definitions. It is up to the user how to define the boundary conditions, therefore the results will be as correct as the user defines them. The physical models employed may also be a source of error. Choosing the right turbulence model, density calculation method or radiation calculations affect the results.

All iterative solvers should run long enough to minimize the numerical error. Solver can be terminated at any time but great attention must be taken for achieving converged results. Default convergence criteria or predefined tolerances do not always assure converged results. Even when the residuals fall below the convergence criteria, more iterations may be needed for the convergence. In order to understand when the results are converging, it is essential to open extra convergence monitors for some scalars in FLUENT. In

our models always 2 additional temperature monitors were opened and they were tracked until the temperature values reach steady values. This is often seen when the residuals fell below 1×10^{-3} down to 1×10^{-4} .

One more important aspect to reduce the error in CFD calculations is to have a grid-independent solution. Grid must be fine enough to capture all flow features and analysis results must not change when the models are run with finer meshes. If the results are changing as the number of cells used are increased, then finer mesh should be created for grid-independency.

For some big models, the mesh resolution at critical locations cannot be transformed to the whole domain. Then non-conformal interface can be used. This is the case where the high density grid in and around the heat sinks is not spread to the whole computational domain. This introduces some error. The reason is that, single cell on one side of the non-conformal interface corresponds to several cells on the other side. So, an interpolation is done at the interface.

If the flow is turbulent then the error increases compared to the laminar case. Since we do not have enough computational resources to solve turbulence with Direct Numerical Simulation we have to model it. This modelling brings another type of error to the solution. There are turbulence models like Large Eddy Simulation, Detached Eddy Simulation or even Reynolds Stress Modelling, but they are far too expensive for our computational resources. Therefore we use Reynolds Averaged Navier Stokes equations to solve for the turbulence.

Comparisons of different discretization schemes, convergence criteria, grid resolution, turbulence models and radiation for temperature distributions on the heat sinks are given next.

3.1.1 Discretization

The first source of error comes from the theory of finite volume method. Interpolations have to be done for discretization. There are numerous schemes for this and the easiest is the first order upwinding. The advantage of this scheme is easy convergence. However, it is only first order accurate. It is suggested to use second order schemes for unstructured grids [31]. In our cases, the comparison of the first order and the second order upwinding schemes is done.

For the flow direction, shown in Figure 3.1, the temperature distributions on the same heat sink, Evercool, which is solved by the first order and the second order upwinding schemes respectively are shown in Figure 3.2. The scale on the left side of the pictures ranges from the local minimum to the local maximum temperature values on the heat sink.

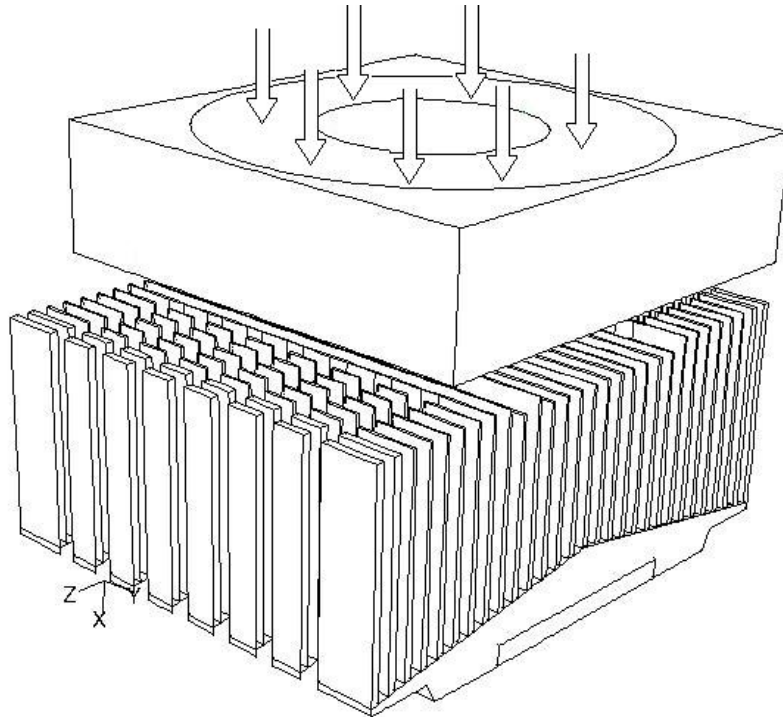
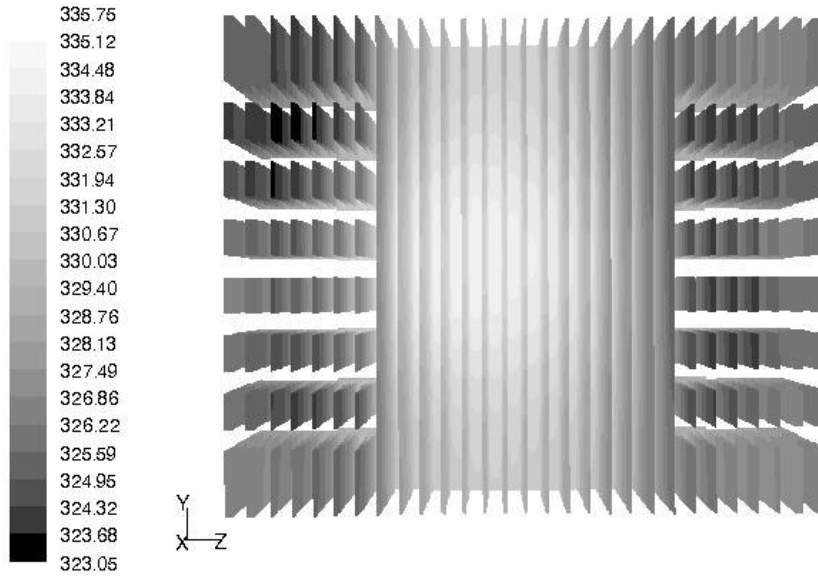
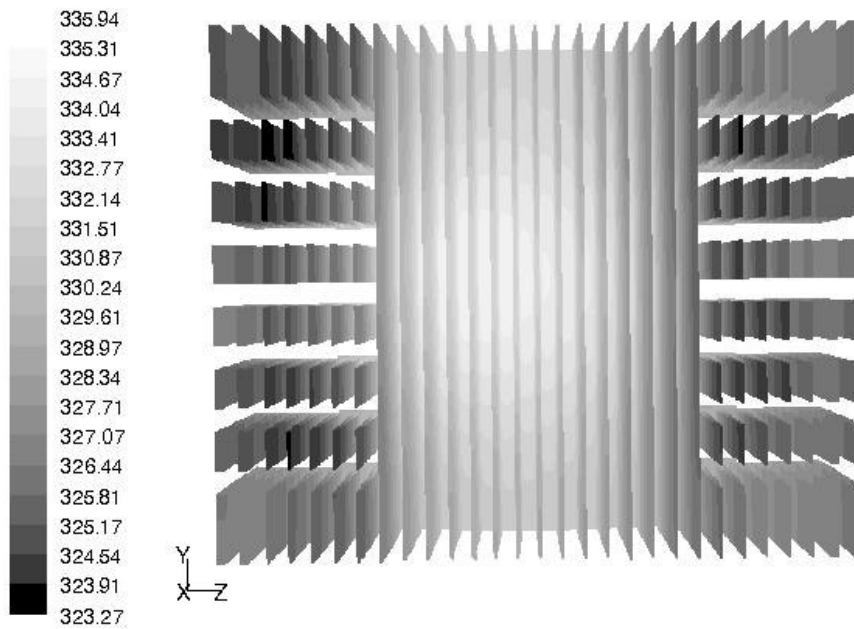


Figure 3.1 Air flow direction shown on heat sink fan assembly.



Contours of Temperature (K)



Contours of Temperature (K)

Figure 3.2 Temperature distributions on Evercool Heatsink for the first order discretization (top) and the second order discretization (bottom) solutions

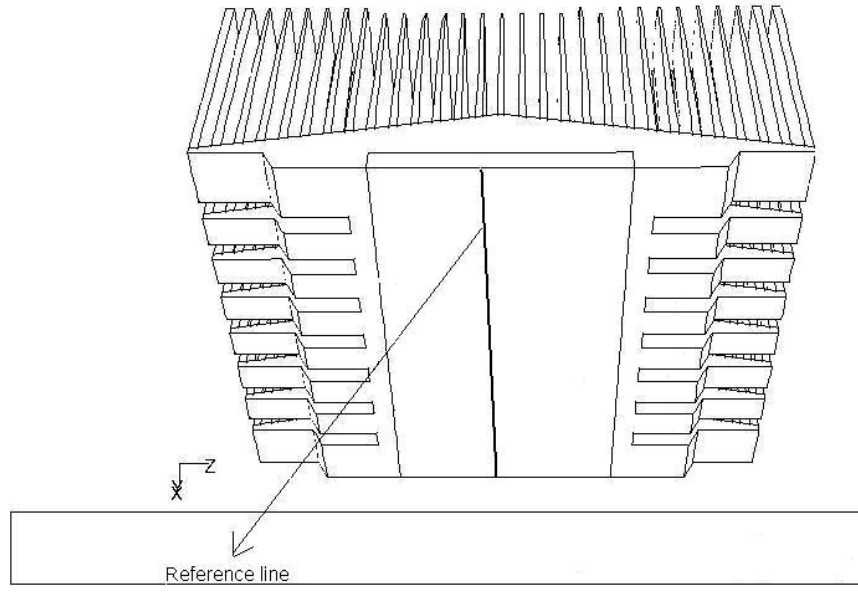


Figure 3.3 Reference line for temperature comparison of different upwinding schemes.

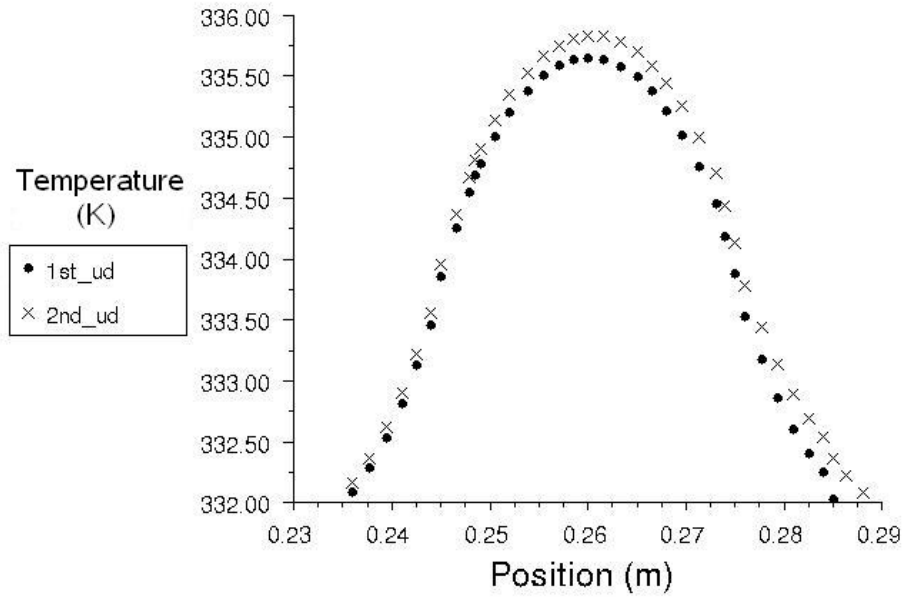


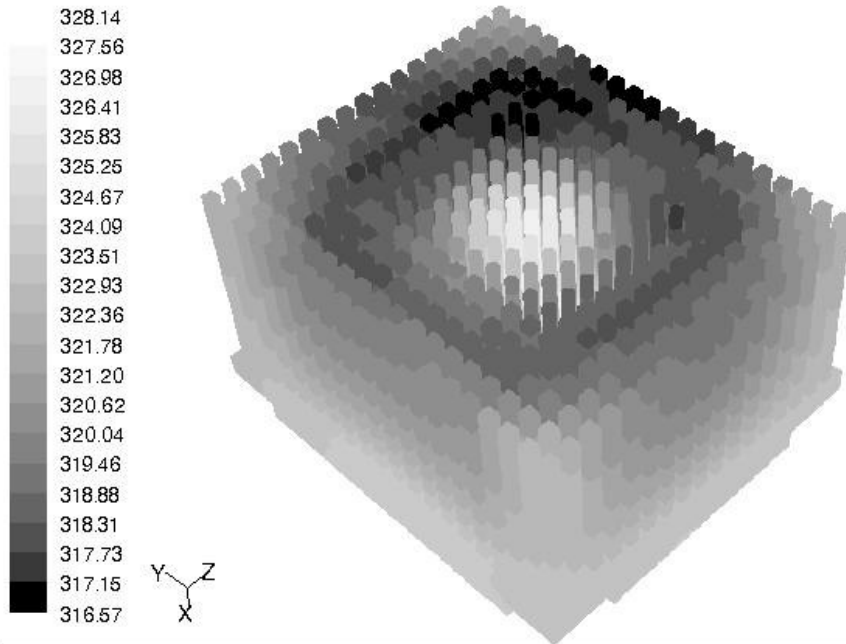
Figure 3.4 Temperature plots on the reference line for two upwinding schemes.

Figure 3.3 shows a reference line on which the temperature plots are taken from the two models; Evercool heat sink converged both with the first order upwinding and with the second order upwinding as shown in Figure 3.4.

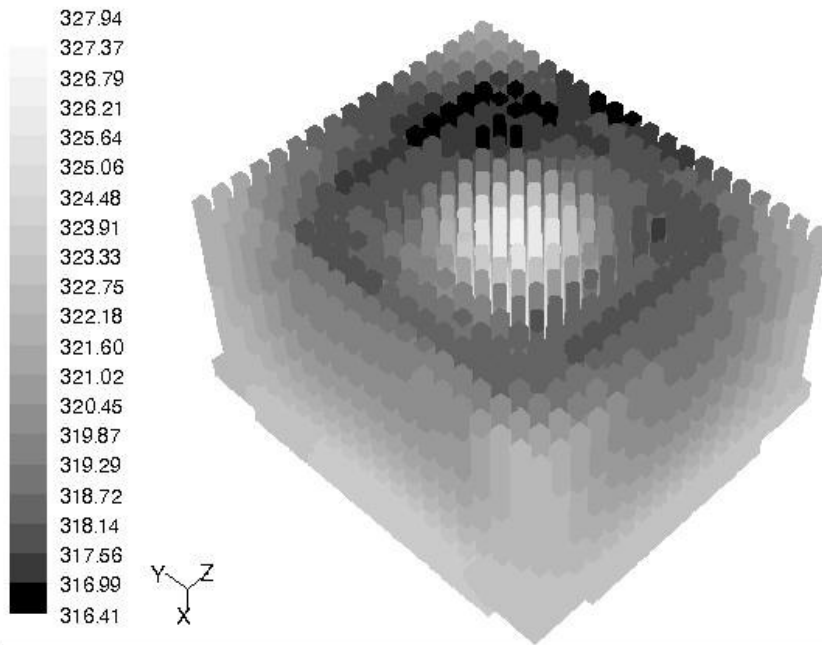
As can be seen, there is a negligible difference between the results of the two schemes. The reason is considered to be the high quality cells forming up the grid and that many of these cells are hexahedral elements which decrease the errors originating from interpolations.

3.1.2 Convergence Issues

Only a well converged, well posed and grid independent simulation can give reliable results. Convergence is determined by the order of magnitude residuals drop. Two different convergence tolerances are compared, one is 10^{-3} for flow and 10^{-6} for energy, and the other is 10^{-4} for flow and 10^{-7} for energy. Running the solver such that residuals fall one more order of magnitude means that more iterations are done to improve the solution quality. It should be noted that, convergence criteria must assure that the results do not change as the iterations proceed. There is a common way of implementing this. Scalar change of some values like temperature is displayed as well as the residual monitors. When the scalar values stay at a certain number and do not change as the iterations continue, then it can be stated that the solution is converged. It was seen that this trend is achieved when the continuity and momentum residuals fell below 10^{-4} and energy residual fell below 10^{-7} . Therefore all the models use the convergence criteria of 10^{-4} for the flow variables and 10^{-7} for the energy.



Contours of Temperature (K)



Contours of Temperature (K)

Figure 3.5 Temperature distributions on Alpha CPU heat sink for different convergence criteria, lower criterion at the bottom.

Figure 3.5 and 3.6 respectively shows the temperature contours and plots on a reference line similar to shown in Figure 3.3.

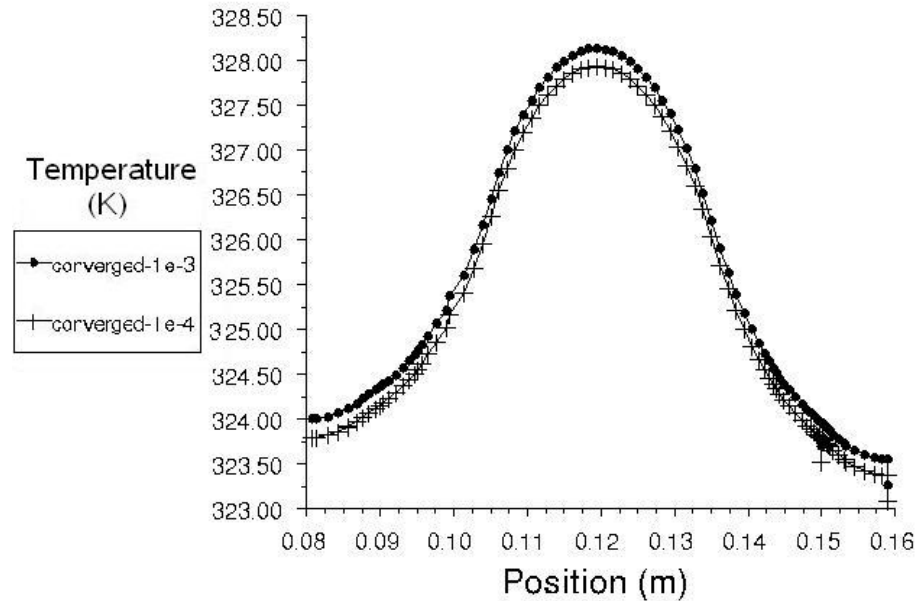


Figure 3.6 Temperature plots on the reference line for two convergence criteria

3.1.3 Grid Independency

The one and only way to establish grid independent solutions is to setup a model with a finer mesh and analyse it to see if there are major differences in scalar quantities and vectors. An additional test case is prepared using 1.5 million cells. The results are compared with the default 900,000 cell model. Figure 3.7 shows the mesh difference for the two models with focus to the heat sink fins. As Figure 3.8 illustrates the temperature distributions are quite similar. This shows that 900,000 cells are enough for the models to be grid independent. Considering that a single analysis lasts for around 20 hours on a Pentium-IV 2.4 GHz computer, it would take unnecessarily more time to have a converged solution with more number of cells, when less could also be good enough.

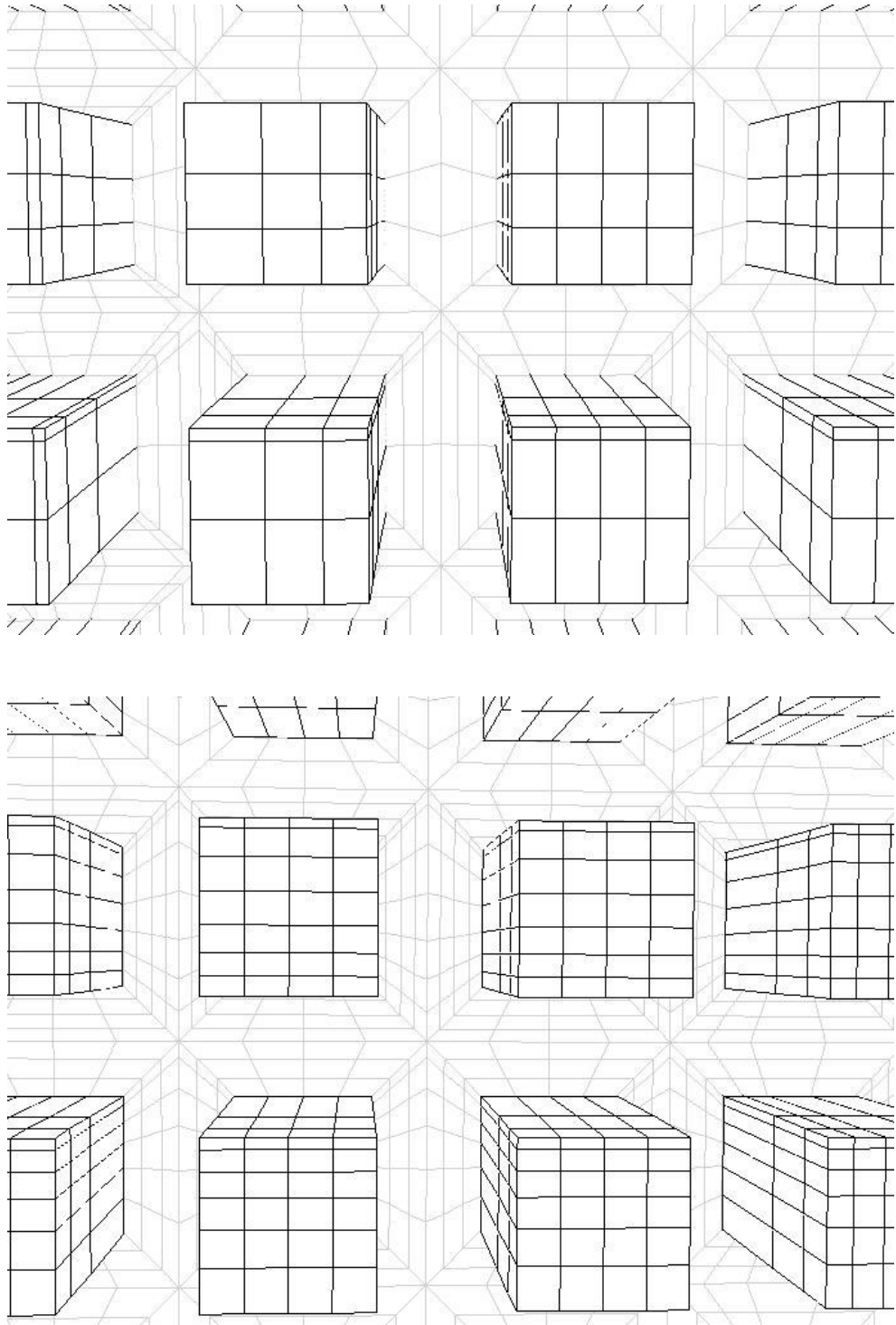


Figure 3.7 Zoom-in picture of mesh resolution on 900,000 cell model at the top and 1.5 million cell model at the bottom.

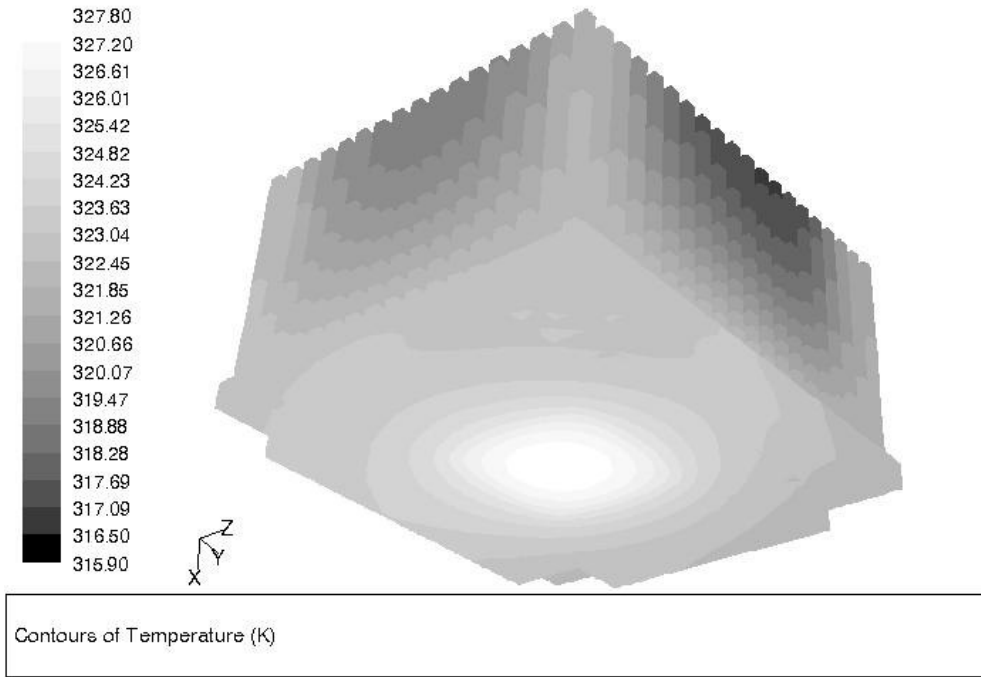
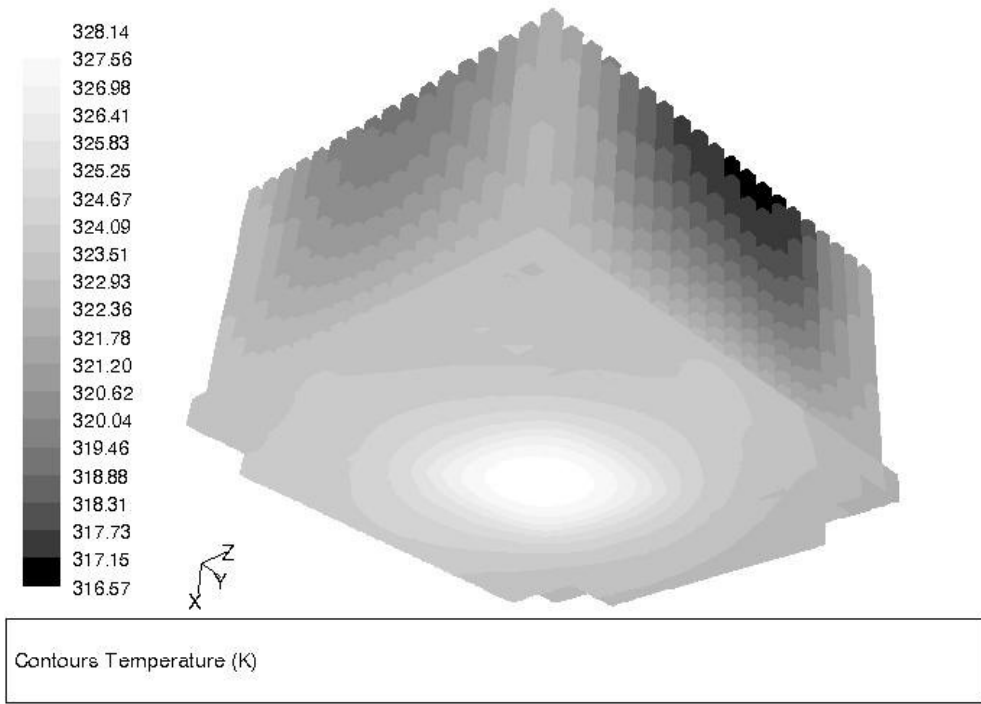


Figure 3.8 Temperature distributions on Alpha Heat Sink for 900,000 cells at the top and 1.5 million cells at the bottom.

Figure 3.9 shows the temperature plots on the reference line for two different grids.

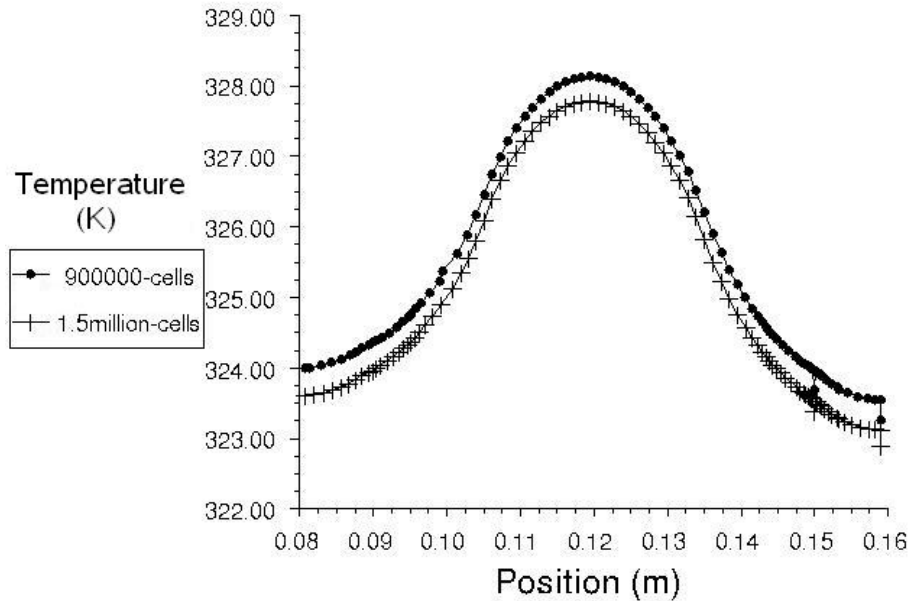


Figure 3.9 Temperature plots on the reference line for two different grids.

3.1.4 Turbulence Modelling

The default turbulence model of all calculations is Algebraic Turbulence Model. It is a zero-equation model and computationally least expensive since no extra equations are solved in addition to continuity, momentum and energy equations. However, in order to rely on the results that algebraic model gives, it should be validated with higher order turbulence models. RNG κ - ϵ model was used as a test case. The temperature distributions and velocity fields are compared. The results show acceptable agreement as seen in Figure 3.10 Therefore it is enough to use the Algebraic Turbulence Model. Using RNG κ - ϵ model, which is a two-equation model, doubles the solution time. This corresponds to two days of continuous runs. The sole reason for that is not the extra equations solved, but also the convergence which is achieved after more iterations.

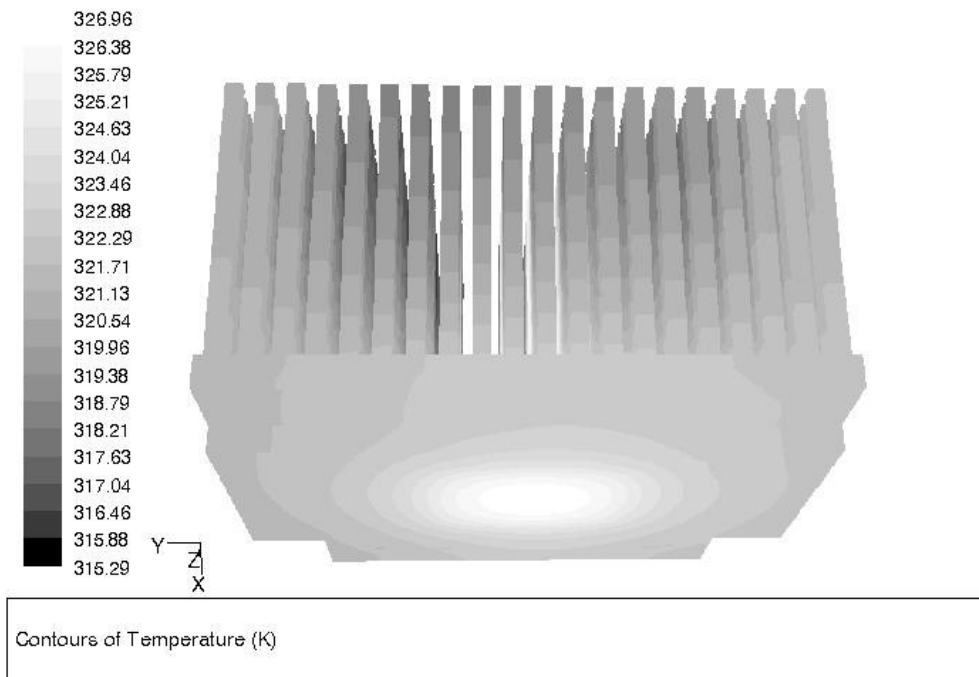
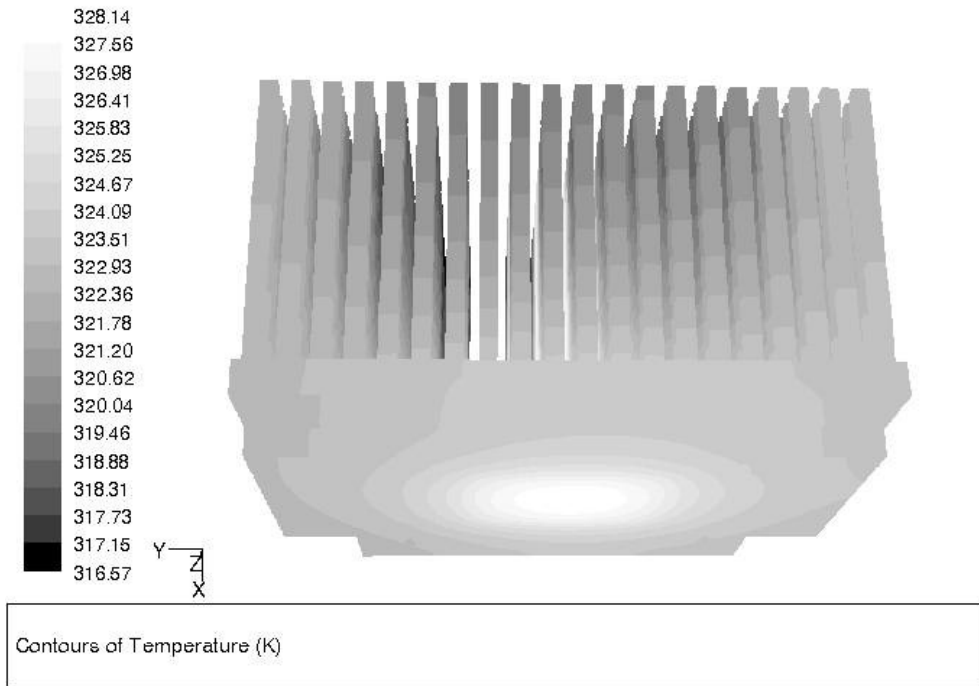


Figure 3.10 Temperature distributions on Alpha heat sink for different Turbulence Models, ATM at the top and RNG κ - ϵ at the bottom

Figure 3.11 shows the difference between the temperatures on the reference line when two different turbulence models are used.

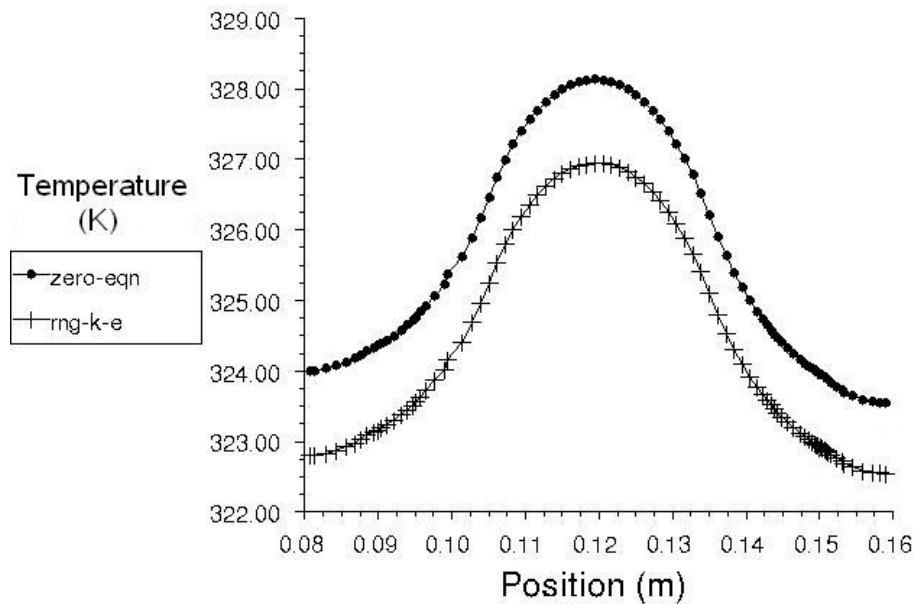


Figure 3.11 Temperature plots on the reference line for the two turbulence models.

3.1.5 Radiation Effects

Alpha heat sink is analysed to investigate the radiation effects. It is known that radiation should be accounted for at natural convection problems and it is not dominant in forced convection applications. In order to decrease the complexity of view factor calculations, some of the objects in the computer chassis are omitted. The computer chassis includes the CPU, CPU heat sink, its fan, power supply and the system fan. Rest of the components are deleted. This model is analysed when radiation is enabled and disabled. The temperature distributions of the two models are almost identical as shown in figures 3.12 and 3.14. Figure 3.13 shows the reference line for which temperature plots are shown in Figure 3.14. Radiation heat transfer helped the Alpha heat sink cool by less than

additional 0.5 K. Therefore it is concluded that radiation could be ignored for forced cooling of electronic devices.

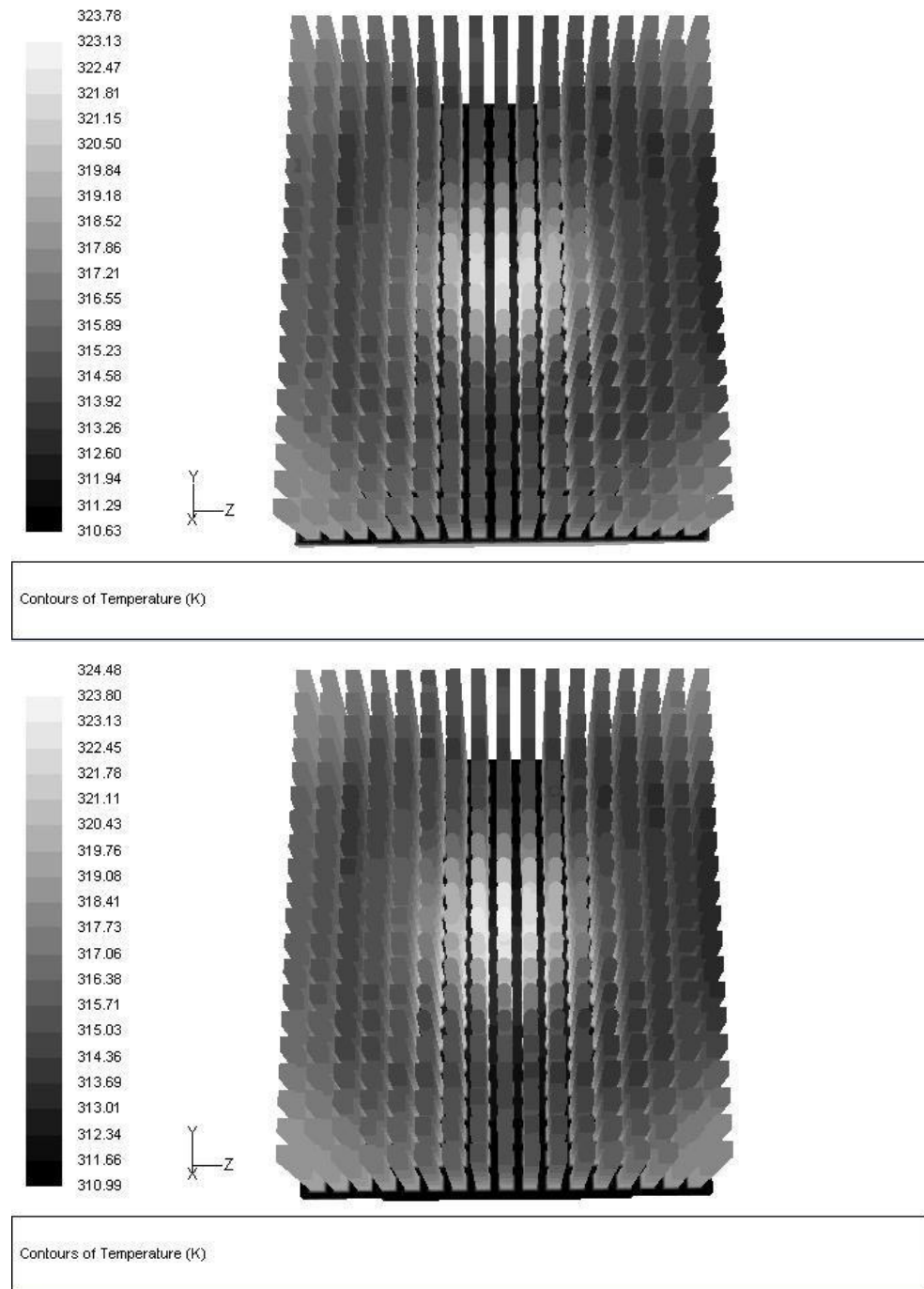


Figure 3.12 Temperature contours for the two models; radiation enabled at the top, disabled at the bottom.

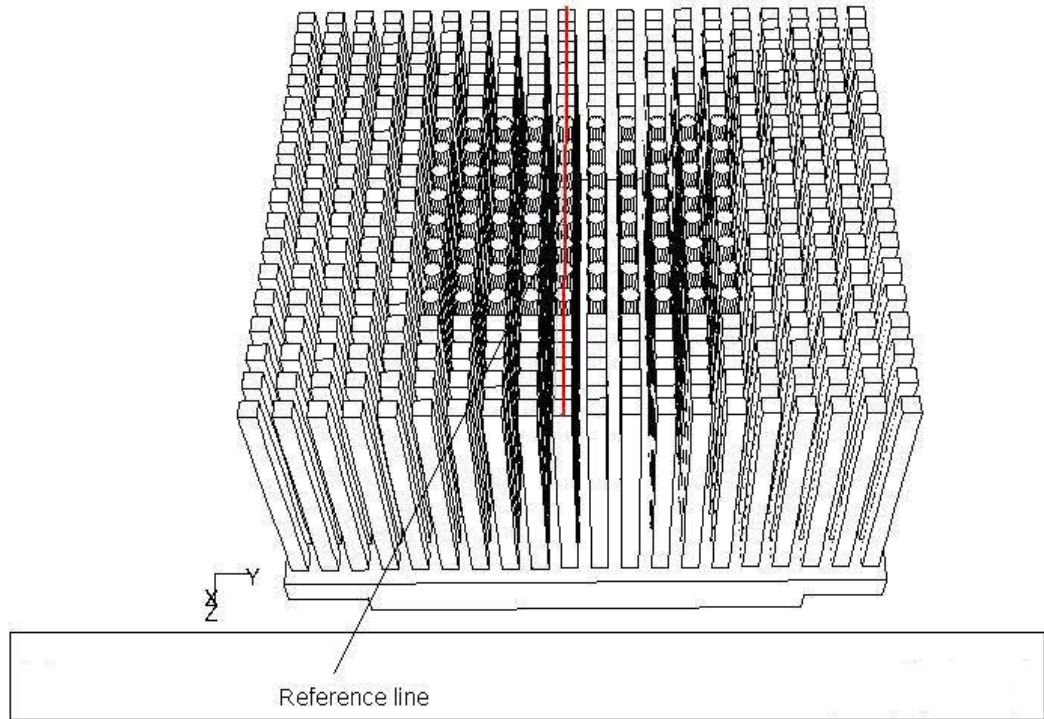


Figure 3.13 Reference line for temperature comparison of radiation heat transfer.

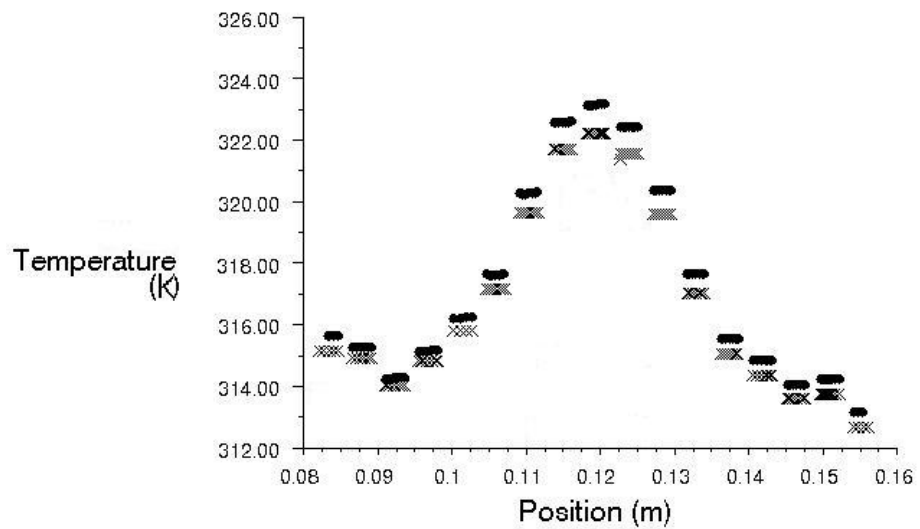


Figure 3.14 Temperature plots on the reference line for radiation heat transfer comparison. Dots for radiation disabled, crosses for enabled.

3.2 Temperature Distributions

For the considered three heat sinks, the temperature distributions are shown in Figure 3.15.

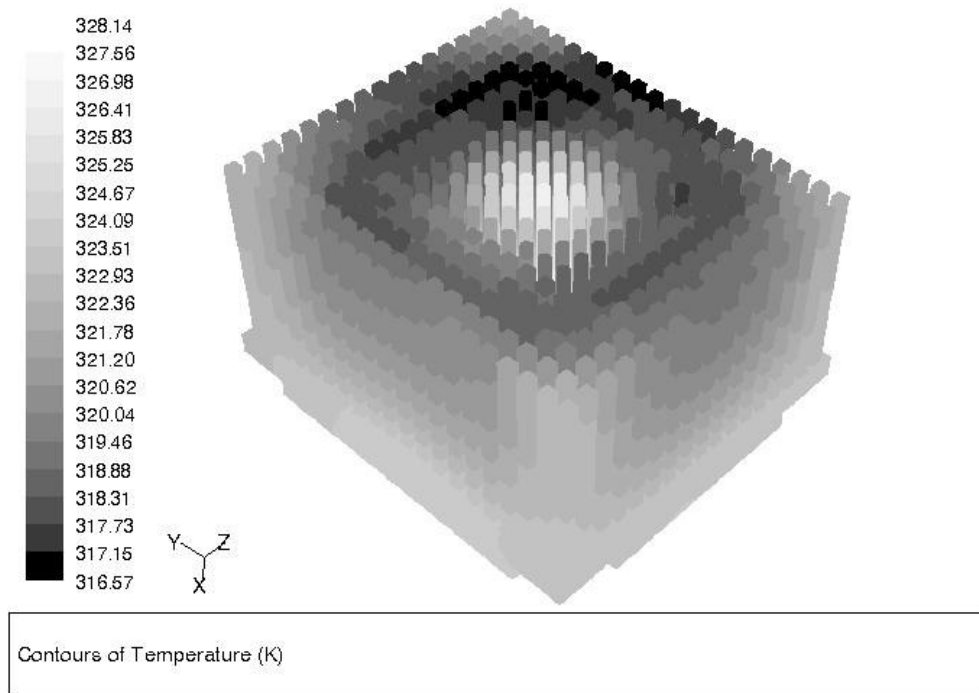
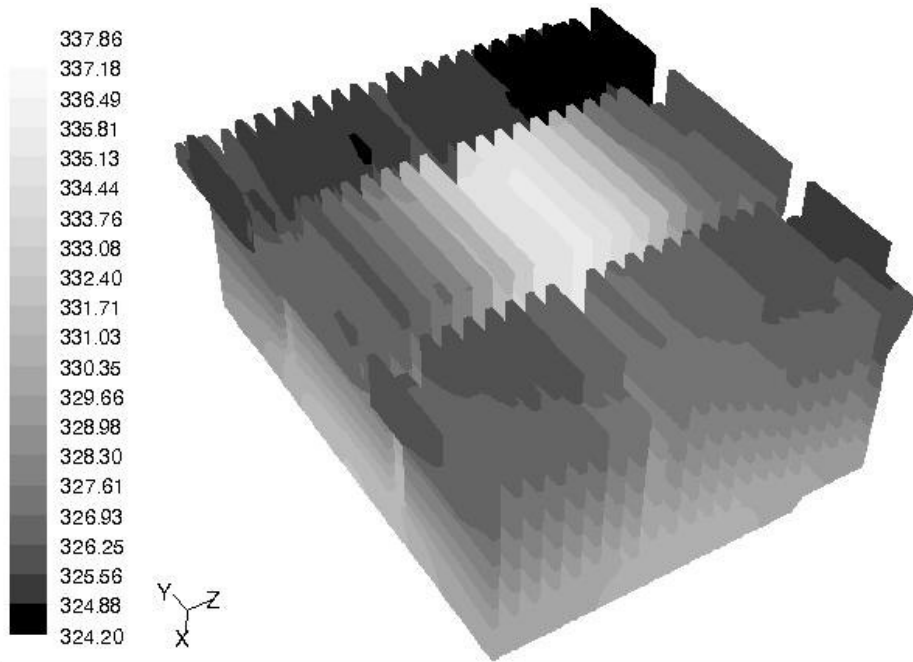
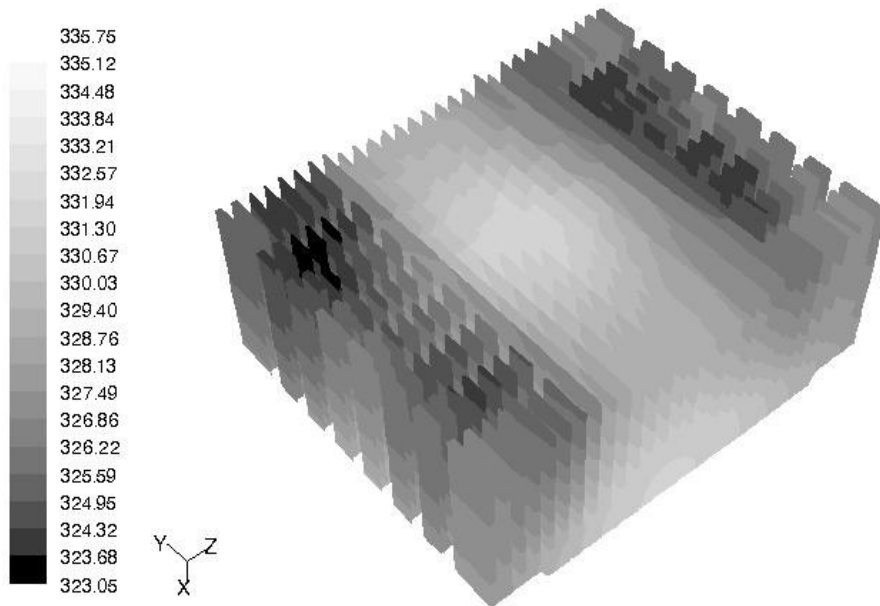


Figure 3.15 Temperature distributions on different CPU heat sinks, from top to bottom, Alpha, Coolermaster and Evercool.



Contours of Temperature (K)



Contours of Temperature (K)

Figure 3.15 (continued)

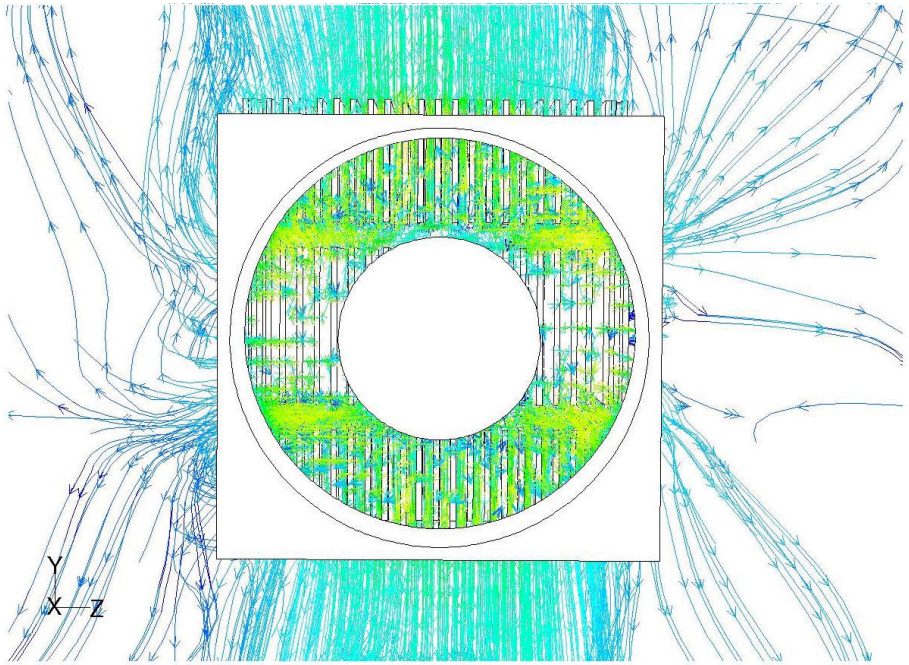
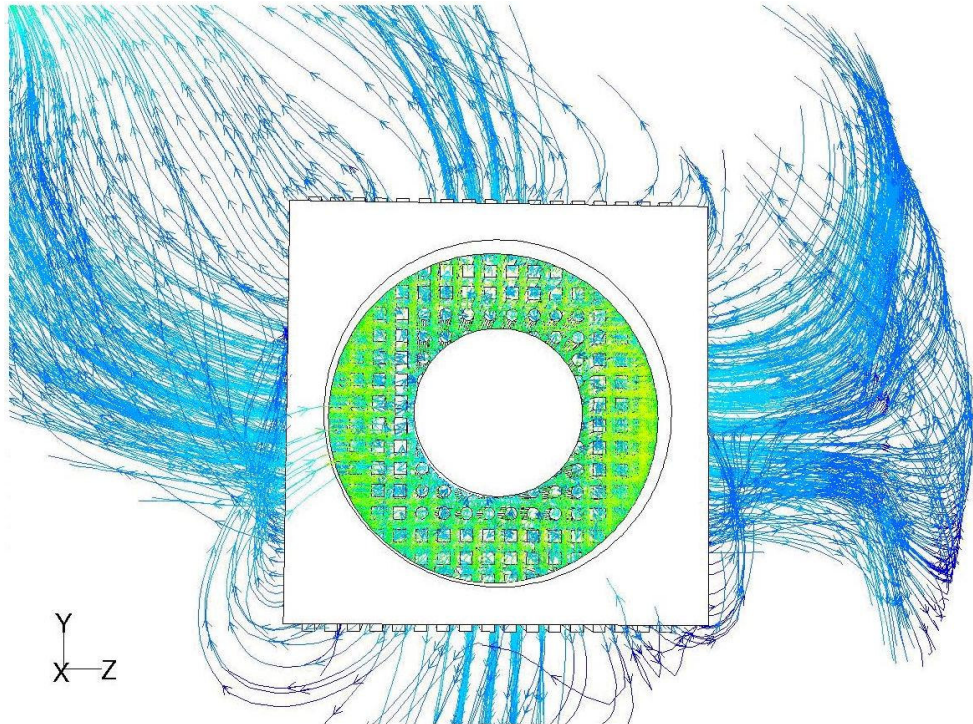
Table 3.1 Maximum and minimum temperatures for the three heat sinks.

	Alpha	Coolermaster	Evercool
T_{\max} (K)	328	338	336
T_{\min} (K)	316	324	323
ΔT	12	14	13

It is obvious from the pictures and the Table 3.1 that, Alpha heat sink outperforms the other two. The main reason for this is that it is a bigger heat sink with more heat transfer area. Evercool performed better than Coolermaster. Although the heat sink dimensions are similar for these two heat sinks, Evercool has a copper embedded base which enables higher conduction rates and heat is conducted to the whole heat sink in a more efficient way. For all heat sinks, it can be stated that the centre of the heat sinks are the hot spots since the heat source corresponds to the proximity of the base centre. The fans installed on the heat sinks are identical with dimensions and fan curves. The fans have hubs where air cannot pass through and it makes the centre parts hotter. In the current simulations, the swirl of the fan is not modelled since the fans are lumped parameter models. For real cases the centre would not be as hot as the simulations predict due to the swirl.

The non symmetric temperature distributions are due to the flow obstructions inside the computer chassis, around the heat sink. The left side of the heat sink is obstructed by the computer chassis walls, whereas on the right side stands the memory cards. Below lies the AGP card. Also at the top there is the power supply, although it is not a solid obstruction since it is modelled as a porous medium, it also blocks the flow. When the computer chassis is investigated, only the upper right part of the heat sink has a free path for the air flow. Therefore air driven by the CPU fan can travel to that side. On the other sides, since the air hitting the walls or other cards return to the proximity of the heat sink, the fan

sucks that relatively hot air and the cooling is less efficient at these sides of the heat sink.



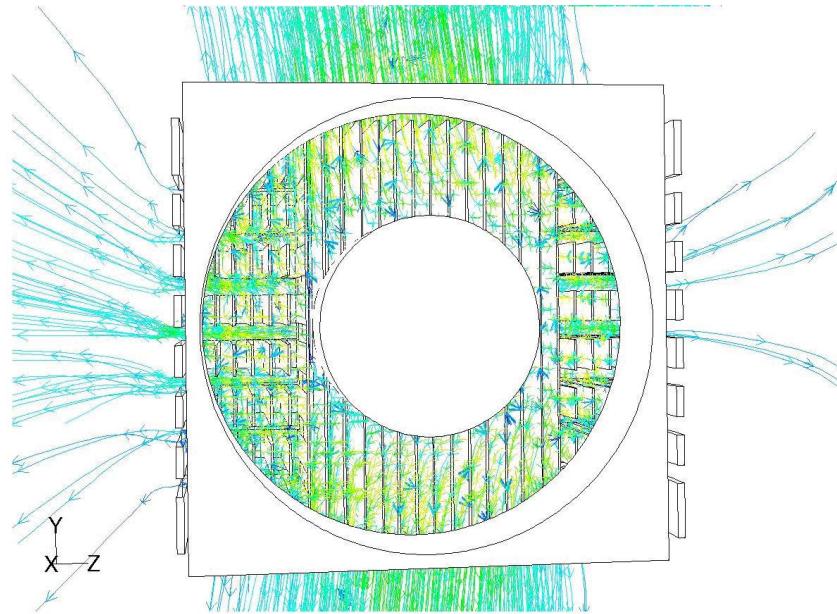


Figure 3.16 Path lines for heat sinks Alpha, Coolermaster and Evercool.
(from top to bottom)

The function of the CPU fan is not only cooling the CPU heat sink but also contributing to the system cooling. Chipset, which is a considerable heat source is not directly cooled by fans. It is cooled by the flow driven by the CPU fan. Although Alpha heat sink performs better than the other ones, it cannot effectively cool the chipset heat sink. When the velocity vectors are investigated through the chipset heat sink at Figure 3.17, the velocity magnitudes at the first heat sink are less than half of the velocity magnitudes at the second and the third heat sinks. This results in an overheating of the chipset. The overheating chipset is the one with Alpha heat sink. The reason why Alpha heat sink's fan can not cool the chipset is seen from the path lines on Figure 3.16. The geometry of Coolermaster and Evercool heat sinks direct the air flow from the fan to the positive and negative y directions, i.e. to the top and the bottom parts of the computer chassis. Less air travels to the sides. This is not the case for the Alpha heat sink. It allows the air to exit from all four sides so the air cooling the chipset

heat sink is less than the others. Also Alpha heat sink is taller than the other which makes the air coming from the heat sink pass higher over the chipset.

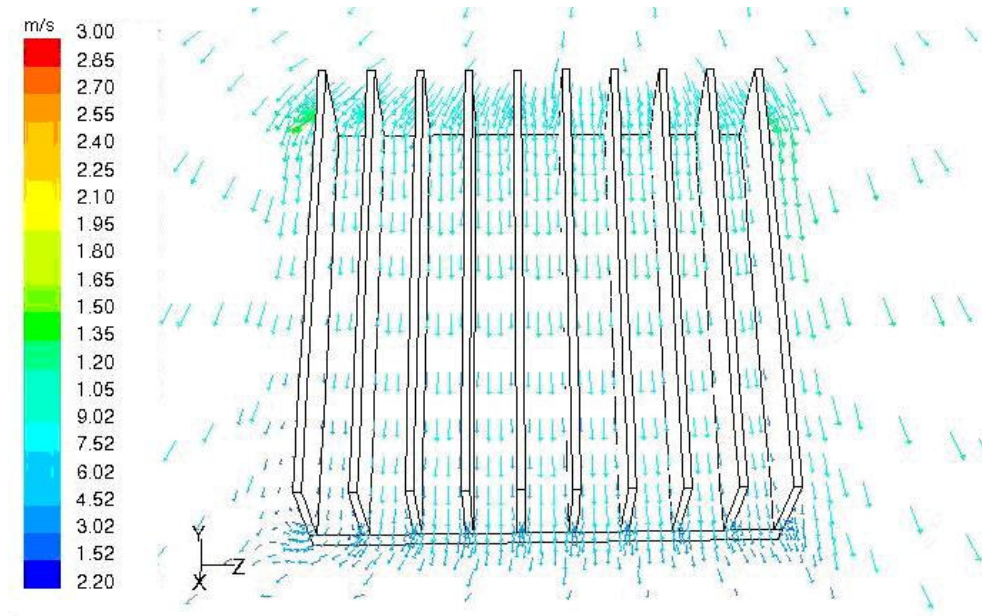
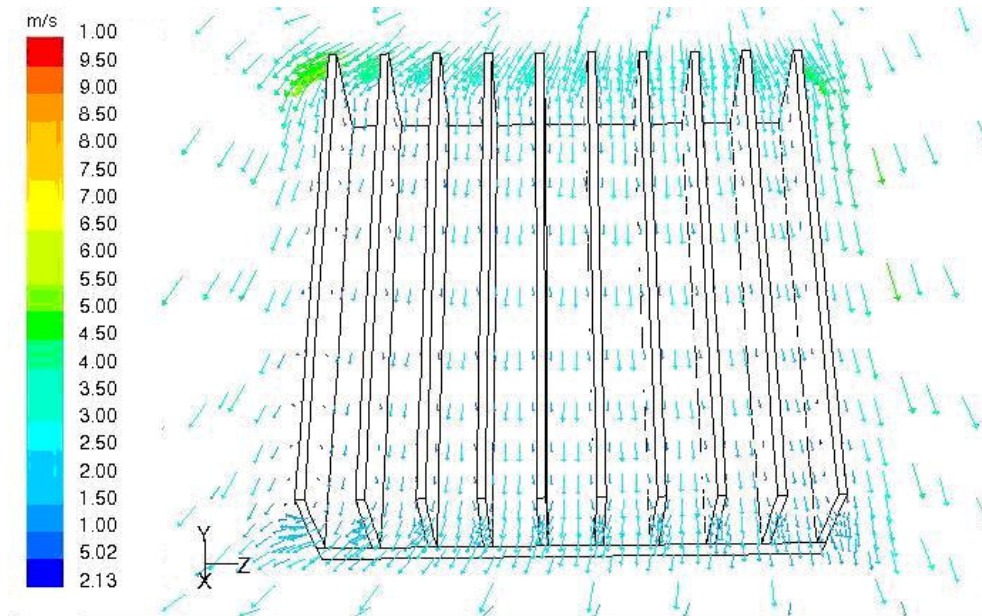


Figure 3.17 Velocity vectors for chipset heat sinks where CPU heat sink is Alpha, CoolerMaster and Evercool from top to bottom.

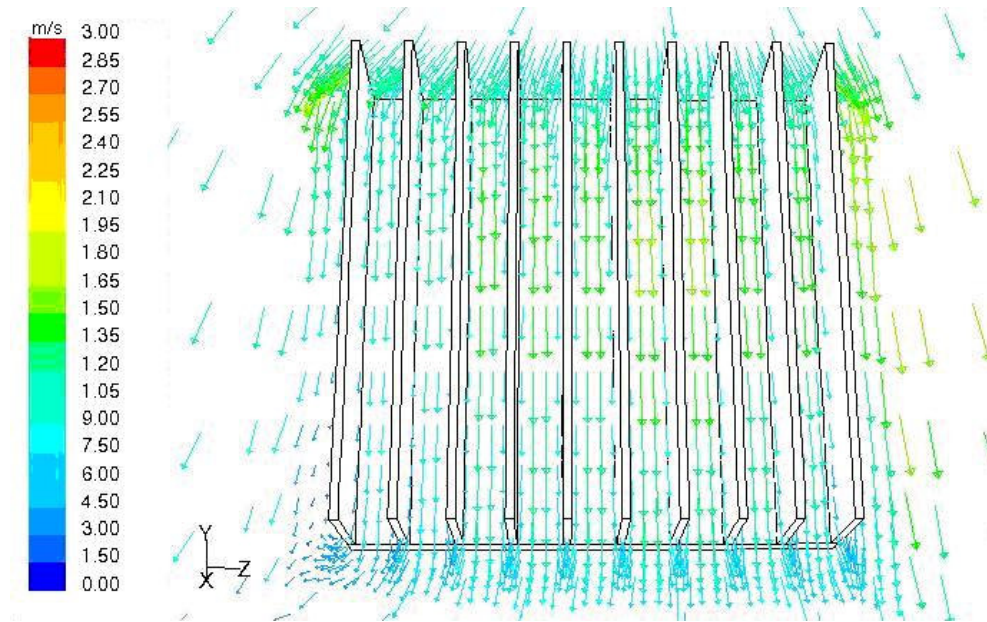


Figure 3.17 (continued)

3.3 Comparison with Experimental Data

There were some experiments in the literature that have been conducted on CPU heat sinks. Among these, the data obtained by Frostytech [35] is used for comparison. Their test setup is not the whole computer chassis system, but some smaller domain in order to simplify the experiments. They have prepared a copper block to install the heat sink over and heated the block with two different heat loads, 50W and 100Ws. Then the rise above ambient temperature values has been recorded. In our simulations, average temperature that the fan blows is calculated. This value is used as the corresponding ambient temperature of the test setup. Since the test setup is an open domain, the ambient temperature is the temperature of the air blown on to the heat sink. However in our simulations, ambient temperature is the temperature outside the domain, so the air blown by the CPU fan is considerably higher than the outside temperature. This necessitates the calculation of average temperature at the fan exit.

Table 3.2 Rise above ambient temperature values (Adapted from [35])

$\Delta T(K)$ Heat Loads	Alpha	Coolermaster	Evercool
50 W	12.0	23.3	19.1
100 W	25.4	34.4	38.5

Table 3.3 Experimental and numerical results

		Alpha	Coolermaster	Evercool
50 W	ΔT Experimental	12.0	23.3	19.1
Experimental Setup	ΔT Numerical	13.1	22.8	17.4
	Error	-7.5 %	1.7 %	8.9 %
100 W	ΔT Experimental	25.4	34.4	38.5
Experimental Setup	ΔT Numerical	27.2	33.9	35.3
	Error	-7.2 %	1.5 %	8.3 %

Although the comparison was made quantitatively, it would be better considered as a qualitative one. For a good quantitative comparison, the test setup should be modelled precisely. However, most of the heat sinks are shipped with their specific fans already installed. These fans have, although close to the ones used in the current simulations, different rotation speeds, different blade geometries and dimensions. Some heat sinks are designed for low thermal resistance whereas some are designed for low noise. Therefore although the test setup is correctly modelled, different fans make it meaningless to compare the heat sink performances. In our models identical fans are used for all three heat sinks. Nevertheless, it was clear both from the experiments and from our analyses that Alpha outperforms the other two heat sinks.

CHAPTER 4

HEAT SINK DESIGN IMPROVEMENTS

4.1 Improvement Cases

Eight different cases were analysed in order to investigate the effects of number of fins, base thickness and heat sink material for improvement purposes. Four cases were investigating the effects of number of fins, two for base thickness and two for heat sink material. Since each run lasts for about 9 hours on a Pentium IV 2.4 GHz, 1GB RAM computer, only a limited number of cases are considered for improvement.

4.2 Number of Fins

When compared with Evercool and Coolermaster heat sinks, Alpha heat sink performed better. However by use of CFD it could be modified to perform even better. When the temperature distributions and the path lines from the fan on figures 3.15 and 3.16 are investigated, it was seen that densely stacked fins do not allow much air to cool the hottest centre parts of the heat sink. So by removing some of the fins a gateway is opened for cool air. 36, 52 and 56 fins are removed successively as shown in Figure 4.1

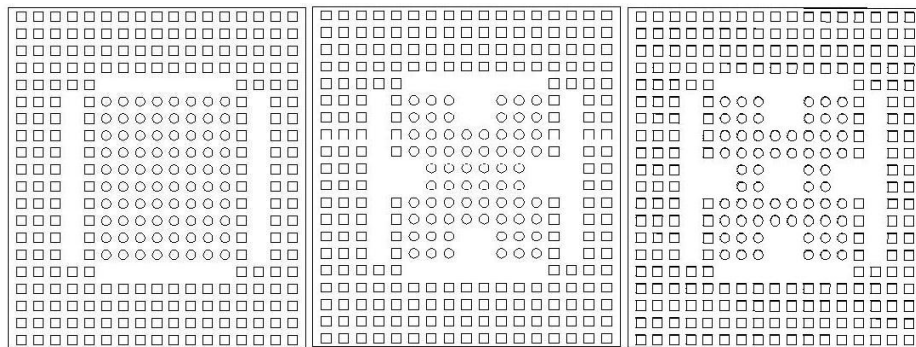


Figure 4.1 Three modified versions of Alpha heat sinks

Table 4.1. Maximum and minimum temperatures on modified heat sinks.

	36 fins less	52 fins less	56 fins less
T_{\max} (K)	328.71	328.94	328.93
T_{\min} (K)	316.03	316.04	316.02
ΔT	12.68	12.90	12.91

From the temperature distributions at Table 4.1, it was seen that removing some of the fins did not affect the performance. The total heat transfer area decreases by removing fins, but due to a better flow path for the air the performance does not change. Although there is not a significant change in thermal resistance, less material can be used which is an improvement for the manufacturer. When even more fins are removed from the heat sink, the temperature on the heat sink increased significantly as shown in figures 4.2 and 4.3.

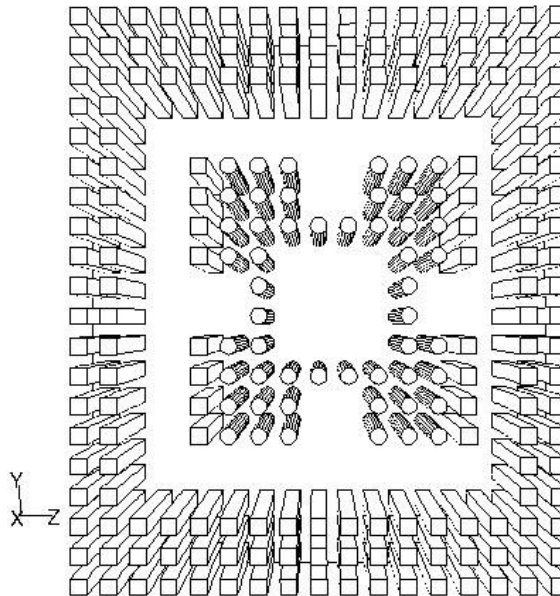


Figure 4.2 Alpha heat sink with fewer fins

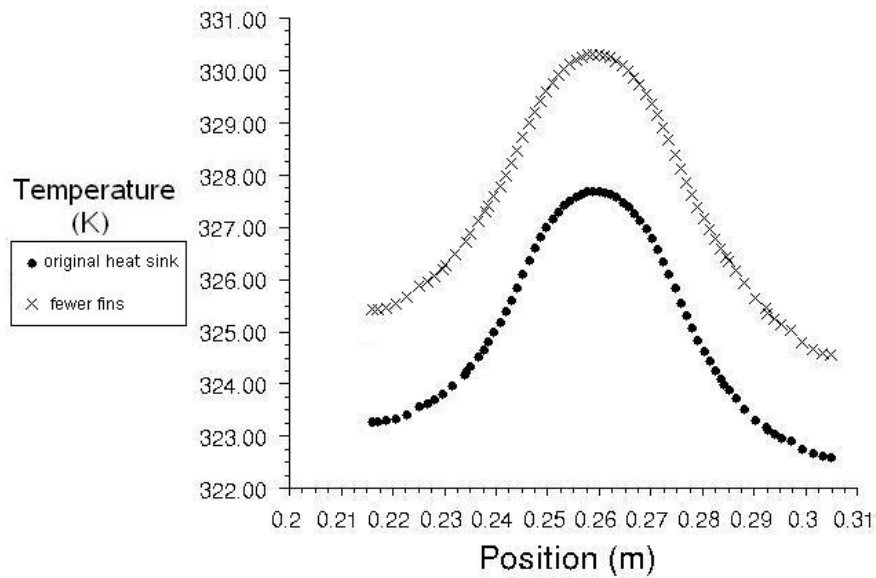


Figure 4.3 Temperature plots on the reference line for the original heat sinks and the heat sinks with fewer fins.

4.3 Heat Sink Material

After taking the improved design after removing 52 fins as a basis, improving thermal conductivity by using copper instead of aluminum is considered. First, it was seen that when the 4 fins at the centre of the heat sink are modified to be copper, the thermal performance of the heat sink was not affected. This also indicates that these fins do not contribute much to the heat transfer. This was expected from the previous analyses where removing the 4 centre fins did not change the temperature distribution. However when all the fins are made of copper, maximum temperature on the heat sinks decreased by 2 °C. It was also seen that the minimum temperature increased by more than 1 °C. Therefore the temperature gradients on the heat sink are less because of high thermal conductivity of copper. The difference between the maximum and minimum temperatures on the copper heat sink is less than 9 °C whereas for the aluminum

heat sink it was around 12 °C. Figure 4.4 shows the temperature plots on the base reference line for the copper and aluminum heat sinks.

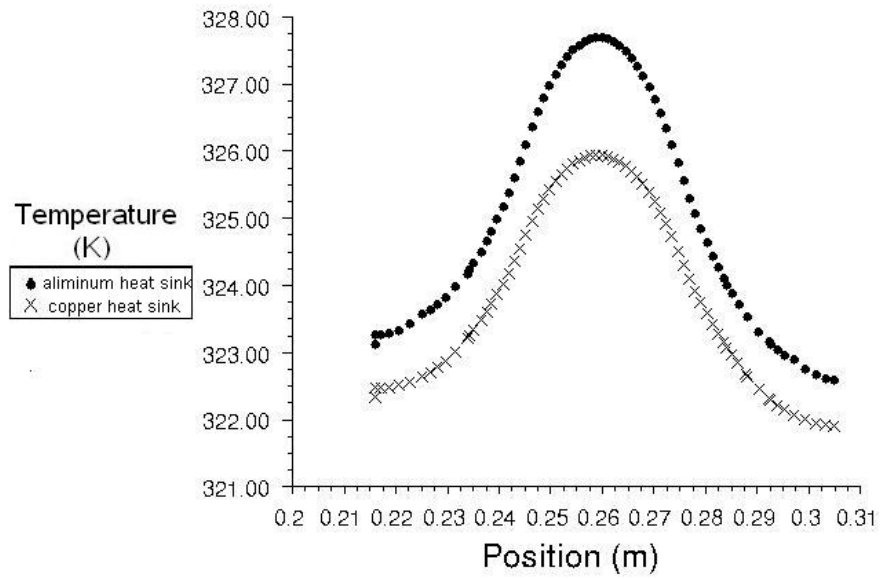


Figure 4.4 Temperature plots on the reference line for heat sink material comparison.

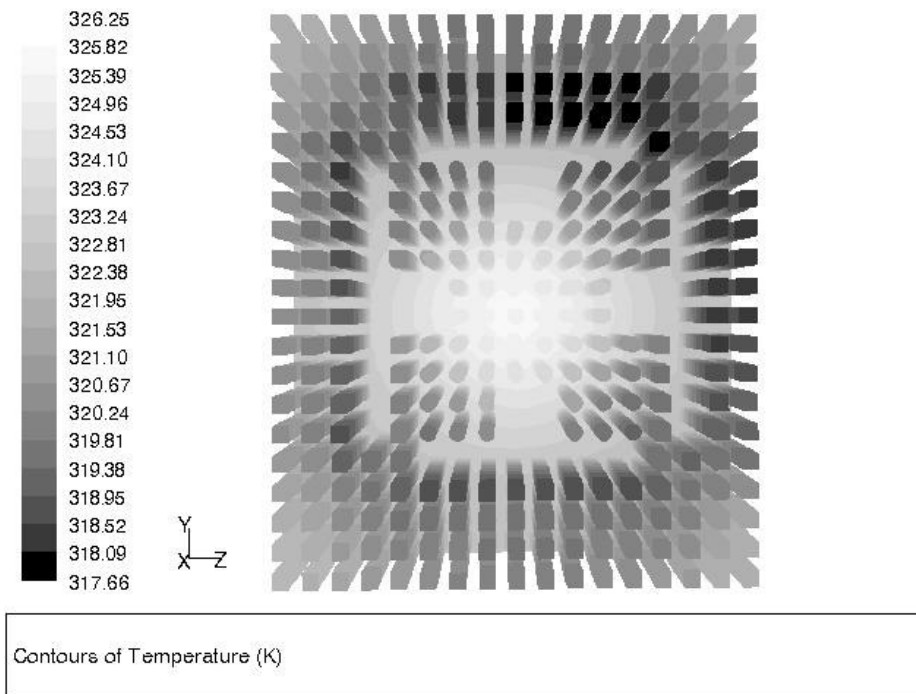


Figure 4.5 Temperature contours on the copper heat sink.

4.4 Base Thickness

In order to investigate the base thickness effect, the base thickness has been increased and decreased by 3 mm respectively keeping the fin length constant for the case where 52 fins are removed from the aluminum Alpha heat sink. The temperature plots on the reference lines have been compared in figure 4.6. The heat sink with the thinner base has higher temperatures. The tip temperatures are very high since there is almost no temperature gradient on the fin along the fin length. This means that longer fins should be used in order to decrease the maximum temperature at the heat sink with higher base thickness. For the heat sinks whose base width is larger than the footprint of the heat source, which is the case here, the in-plane conduction resistance should be considered. Therefore thicker base thicknesses decrease this resistance. On the other hand, if the heat source and heat sink have the same width it is better make the base thinner to decrease the conduction resistance from the base to the fin tip direction.

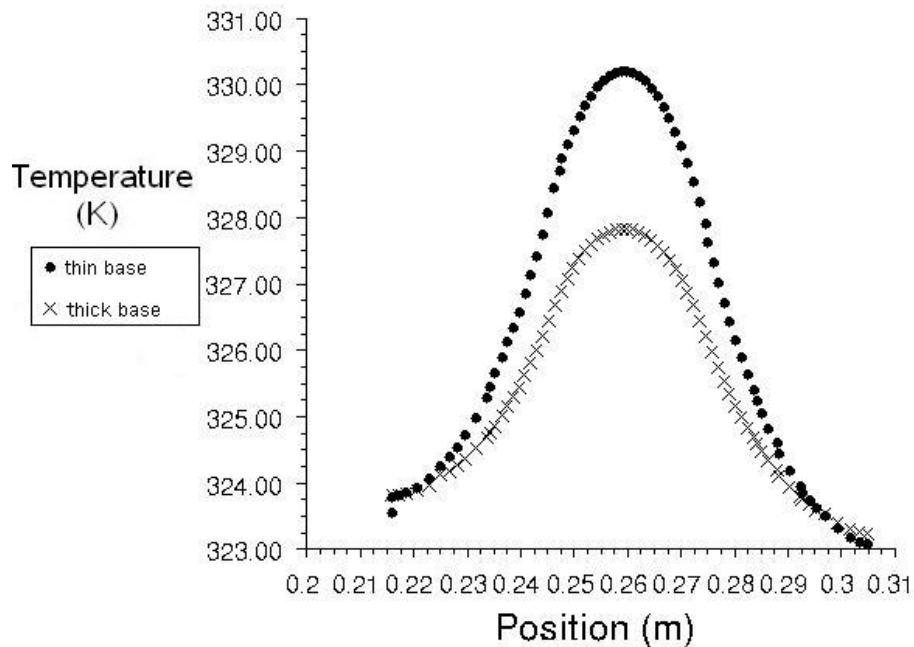


Figure 4.6 Temperature plots on the base reference line for heat sinks with different base thicknesses.

CHAPTER 5

CONCLUSIONS

In this study, CPU cooling has been investigated in a complete computer chassis with different heat sinks and the performances of the heat sinks are compared. A road map has been developed for simulating the computer chassis. The mesh resolution, turbulence model choice, convergence criteria and discretization schemes are investigated to find the best model with least computational expense. This road map is then applied for different heat sink geometries and the comparison of the heat sink temperature difference results were made with the available experimental results. The numerical methods showed agreement with the experimental data. However, the comparison was qualitative. In order to make better comparisons, the experiments should be performed on a computer chassis considering the full model. In this study, since it is not feasible to model the fans and resistances with their exact geometry, lumped parameter models are used. This always introduces some error. Also the environment outside the computer chassis is not modelled; therefore there is one more approximation, for the heat transfer outside the chassis.

The road map for investigating the heat transfer in a computer chassis suggests that:

- Mesh should be generated such that 3 cells in the narrowest air gap and 2 cells in conduction zones are enough. More mesh distorts the stability of the model with the penalty of more run times.
- Non-conformal mesh can be used so that the fine mesh parameters are stored inside the non-conformal mesh interfaces where heat sinks are located. This prevents the generation of excessively many cells which increases the computational cost. If the analysis

is going to be running on a single computer instead of a parallel cluster, non-conformal mesh is compulsory.

- First order discretization scheme is enough if the grid is dominated by hexahedral cells. Convergence is faster with this scheme.
- Zero-equation turbulence model is suitable for analysing fluid flow and heat transfer in a computer chassis. Higher order turbulence models are unnecessarily expensive.
- Radiation effects can be ignored due to the domination of forced convection and relatively low temperature differences inside the chassis.
- Convergence must be assured by checking the residuals and also the temperature monitors. It is necessary to let the residuals to drop more than three orders of magnitude.

Experimental verification is important for CFD analyses. Verification of a base model can be a reference for the consequent simulations.

Improvements on heat sink designs is possible via CFD. Number of fins and their distribution, fin material and base plate thickness can be investigated and thermal enhancements may be succeeded as well as material saving. Successive parametric runs are necessary to be able to evaluate the effects of these design parameters. Eventually it is possible to end up with a new heat sink design which has better thermal performance and uses less material. In the current study, it was seen that stacking too many fins is not a solution for decreasing the hot spots on the heat sink since they may prevent the passage of air coming from the fan to the hottest centre parts of the heat sink. If fin material is selected to be copper rather than aluminum, then the thermal resistance of the heat sink decreases as expectedly. However this makes the heat sink more expensive and heavier. The heat sink base thickness is also a parameter for improvement. In our cases, the footprint of the heat source is smaller than the width of the heat sink which

introduces an in-plane conduction resistance. When the base plate thickness is increased the heat sink performed better, however there are space limitations for every heat sink in a computer. Therefore the total height of the heat sink should be considered together with the space limitations when increasing the height of the heat sink. Designing a narrower heat sink to decrease the in-plane conduction resistance is not a solution since it can accommodate fewer fins on itself which decreases the total heat transfer area.

Finally it was seen that even very complicated geometries can be modelled for the solution of conjugate heat transfer using CFD and the results are acceptable as long as attention has paid on mesh density and quality, boundary conditions, convergence quality, physical models like turbulence and discretization schemes.

The current limitations on computer technology have prevented us to model the problems with fewer approximations. That is, it is not possible to solve the Navier-Stokes equations with Direct Numerical Simulation or even without using any lumped parameter model. However, CFD is a useful tool even with these capabilities. It decreases the design time by minimizing the trial-and-error cycle and therefore reducing the cost. A prototype manufactured after every trial is the biggest source of time loss which can be reduced by use of CFD. There are cases where prototyping and experimental study is not possible especially in avionics. There is no chance to try a prototype whether it works or not on an aircraft. So new applications of numerical methods are emerging day by day and this study is one of the first to analyse the whole computer chassis.

REFERENCES

- [1] Dave S. Steinberg, "Cooling Techniques for Electrical Equipment," Second Edition, John Wiley & Sons, 1991.
- [2] Richard C. Chu, Foreword to "Air Cooling Technology for Electronic Equipment," CRC Press, 1996.
- [3] Seri Lee, "Optimum Design and Selection of Heat Sinks," Eleventh IEEE SEMI-THERM Symposium, pp. 48-54, 1995
- [4] Christopher L. Chapman, "Thermal Analysis Software Picks Optimum Heat Sink Design," IEEE, pp. 37-42, 1997.
- [5] Jinny Rhee, Kaveh Azar, "Adjusting Temperatures for High Altitudes," Electronics Cooling Magazine, September 1999, Vol. 5, No 3.
- [6] Kim Fowler, "Heat Transfer and Cooling," IEEE Instrumentation & Measurement Magazine, pp 48-51, 2001.
- [7] Overclockers web site, www.overclockers.com, July 2003.
- [8] Frank P. Incropera, David P. Dewitt, "Fundamentals of Heat and Mass Transfer," Fourth Edition, John Wiley & Sons, 1996
- [9] Christopher L. Chapman, Seri Lee, Bill L. Schmidt, "Thermal Performance of an Elliptical Pin Fin Heat Sink," Tenth IEEE SEMI-THERM, pp.24-31, 1993.
- [10] K.K. Sikka, K.E. Torrance, C.U. Scholler and P.I. Salanova, "Heat Sinks with Fluted and Wavy Fins in Natural and Low-Velocity Forced Convection," Inter Society Conference on Thermal Phenomena, pp. 149-156, 2000
- [11] P. Sathyamurthy, P.W. Runstadler, S. Lee, "Numerical and Experimental Evaluation of Planar and Staggered Heat Sinks," Inter Society Conference on Thermal Phenomena, pp. 132-139, 1996.
- [12] A. Dvinsky, A. Bar-Cohen, M. Strelets, "Thermofluid Analysis of Staggered and Inline Pin Fin Heat Sinks," Inter Society Conference on Thermal Phenomena, pp. 157-164, 2000.
- [13] Alpha Company Ltd, <http://www.micforg.com>, July 2003.

- [14] Roy W. Knight, Donald J. Hall, John S. Goodling, Richard C. Jaeger, "Heat Sink Optimization with Application to Microchannels," IEEE Transactions on Components, Hybrids, and Manufacturing Technology, Vol 15, pp.832-842, 1992.
- [15] Michael B. Kleiner, Stefan A. Kühn, Karl Haberger, "High Performance Forced Air Cooling Scheme Employing Microchannel Heat Exchangers," IEEE Transactions on Components, Packaging, and Manufacturing Technology-Part A. Vol 18, pp.795-804, 1995.
- [16] Mike Turner, "All You Need To Know About Fans," Electronics Cooling Magazine, May 1996, Vol.2, No 2.
- [17] Robert E. Simons, Roger R. Schmidt, "A simple Method To Estimate Heat Sink Airflow By Pass," Electronics Cooling Magazine, May 1997, Vol.3, No 2.
- [18] Christopher Chapman, Vivek Mansingh, Parbhu Sathyamurthy, "Fan Heat Sinks for High Performance Socket ICs," Icepak Articles, <http://www.icepak.com/news/articles/art6.htm>, November 2002.
- [19] Anandtech, <http://www.anandtech.com/showdoc.html?i=1532&p=3>, January 2002.
- [20] Dave Smith, "General Fan Performance Guide," AMD Articles, <http://www.amdmb.com/print-article.php?ArticleID=132>, September 2001.
- [21] Miksa deSorgo, "Thermal Interface Materials," Electronics Cooling Magazine, September 1996, Vol. 2, No 3.
- [22] M.M. Yovanovich, J.R. Culham, P. Teertstra, "Calculating Interface Resistance," Electronics Cooling Magazine, May 1997, Vol. 3, No 2.
- [23] Robert J. Moffat, "Getting the most out of your CFD program," IEEE Inter Society Conference on Thermal Phenomena, pp 9-14, 2002.
- [24] Masud Behnia, Wataru Nakayama, Jeffrey Wang, "CFD Simulations of Heat Transfer from a heated module in an air stream: Comparison with experiments and a parametric study," IEEE Inter Society Conference on Thermal Phenomena, pp 143-151, 1998
- [25] C-W. Yu, R.L.Webb, "Thermal Design of a Desktop computer system using CFD analysis," Seventeenth IEEE Semi-Therm Symposium, pp. 18-26, 2001.
- [26] Rebecca Biswas, Raghu B. Agarwal, Avijit Goswami, Vivek Mansingh, "Evaluation of airflow prediction methods in compact electronic enclosures," Fifteenth IEEE Semi-Therm Symposium, pp. 48-53, 1999.

- [27] Christopher W. Argento, Yogendra K. Joshi, Micheal D. Osterman, "Forced Convection Air-Cooling of a commercial electronic chassis: An Experimental and Computational Case Study," IEEE Transactions on Components, Packaging, and Manufacturing Technology-Part A, pp. 248-257, Vol.19, No 2, 1996.
- [28] Ronald L. Linton, Dereje Agonefer, "Coarse and detailed CFD modelling of a finned heat sink," IEEE Transactions on Components, Packaging, and Manufacturing Technology-Part A, pp. 517-520, Vol.18, No 3, 1995.
- [29] P. Sathyamurthy, P.W. Runstadler, "Numerical and Experimental Evaluation of Planar and staggered heat sinks," IEEE Inter Society Conference on Thermal Phenomena, pp.132-139, 1996.
- [30] Valerie Eveloy, Peter Rodgers, M.S.J. Hashmi, "Numerical prediction of electronic component heat transfer: An industry perspective," 19th IEEE Semi-Therm Symposium, pp.14-26, 2003.
- [31] FLUENT 6.1 Users Guide
- [32] J.H. Ferziger, M. Peric, "Computational Methods for Fluid Dynamics," Third Edition, Springer-Verlag, 2002.
- [33] H. K. Versteeg, W. Malalasekera, "An Introduction to Computational Fluid Dynamics, The finite Volume Method," Longman Scientific & Technical, 1995
- [34] P. R. Spalart, "Strategies for Turbulence Modelling and Simulations," International Journal of Heat and Fluid Flow 21, pp. 252-263, 2000.
- [35] Frostytech, www.frostytech.com, Heat Sink Reviews, June 2004.
- [36] R. L. Panton, "Incompressible Flow," John Wiley and Sons, 1984.
- [37] A.F. Mills, "Heat Transfer," Second Edition, Prentice Hall, 1999.

APPENDIX A

DETAILS OF THE MODEL

The model studied consists of following objects:

Computer chassis: It defines the computational domain. No mesh is generated outside the computer chassis. Some non-critical parts of the computer chassis are not meshed and modeled by hollow blocks. In our model, natural convection from the computer chassis walls is also considered. For this reason heat transfer coefficient for the horizontal and vertical walls are calculated by lumped parameter methods. This heat transfer coefficient is applied as a boundary condition on the walls. The openings for grilles and fans are also placed on the walls, whose boundary conditions override the wall boundary conditions.

CPU: It is the main heat source in the model. The CPU is modeled as a 2-dimensional area, which dissipates 70W for each model. The CPU dimensions are equivalent to a commercially available CPU, i.e. AMD 2000+.

CPU Heat sink: The most important object in the computer chassis is the heat sink. Various models have been created for investigation of cooling characteristics of different heat sinks. In every model, only the heat sink geometry is changed, all the other objects remained unchanged. This is the most complicated object of all models; therefore it takes more time to create this geometry. Since there is no CAD geometry available, some models are created by measuring the dimensions of the actual heat sink and/or by using the dimensions given by the manufacturers.

CPU Fan: The fan is modeled as a lumped parameter model. It does not have geometrically defined blades. Only the fan curve is defined from which the operating point is calculated.

CPU socket: It is the plastic part on which the CPU is mounted.

AGP: It is the graphics card, which is also a considerable heat source. Therefore it has a heat sink and a fan cooling it. AGP is modeled as a 2D source like the CPU.

AGP Heat sink: It is a simple extruded aluminum channel heat sink. The heat sink is much smaller than the one on the CPU, since the heat dissipated by the AGP is much less than the heat CPU dissipates.

AGP fan: A sucking fan with a linear fan curve is placed on the AGP Heat sink.

Chipset: It is one of the main heat sources on the mainboard. A heat sink is mounted on the chipset, but there is no fan on it, making it a passive heat sink. However it does not work like a passive heat sink since the airflow in the chassis makes it forced cooled. Compared to the CPU, chipset can withstand to higher temperatures.

Main board: It is the main card on which the CPU, chipset and other cards are placed. It is modeled with its thickness. The material of main board is FR4 and copper.

RAM: Two RAM cards are placed on the mainboard. They are also heat sources and the spacing between these two cards is critical. This spacing consideration is out of context of this study, so a fixed, typical spacing is used for all models.

Other cards: Other miscellaneous cards are also modeled. Since there are a lot of very small electronic components on these cards, the cards are also heat sources. The details of these cards are not modeled but, for each case, a heat dissipation is added and distributed to the whole card.

Power supply: Power supply is an important heat source in the case. Also it affects the air flow in the domain. However it is not feasible to model it exactly. Instead, lumped parameter models are used. The power supply with all the inner components, cables and small openings on the outer walls are modeled as a single object, which is a resistance. The 3D fan placed behind it, is the main fan of the computer case.

Grilles: The computer cases have small holes on them, which make air inlet or outlet possible. Since modeling these holes make the model computationally expensive, lumped parameter models are used again. They act like resistances to the flow according to the specified free area ratios.

Floppy and Hard Drives: CD-Rom, DVD-Rom, Diskette Drive and Hard Disk are also modeled. They are modeled as 3D blocks with heat dissipation. Although they may be neglected when their heat dissipation rates are considered, but since they affect the air flow in the system, they are included.

APPENDIX B

MESH GENERATION

The second part of pre-processing is the mesh generation. Mesh is the key component of a high quality solution. Icepak offers three kinds of meshing algorithms. These are Hexahedral Cartesian, Hexahedral Unstructured and Tetrahedral meshers. Hexahedral Cartesian mesher is the one generating fully structured meshes. It is suitable for very limited type of geometries. It is generally inappropriate for models where curved surfaces exist. Hexahedral Unstructured mesher creates grids of hexahedral cells dominantly and tetrahedral cells where necessary. Tetrahedral mesher is designed for very complicated geometries where the other two cannot be used. For models involving spheres or ellipsoids hexahedral meshers are useless. In our problem hexahedral unstructured mesher is used. Figures B.1, B.2 and B.3 show the mesh in the domain.

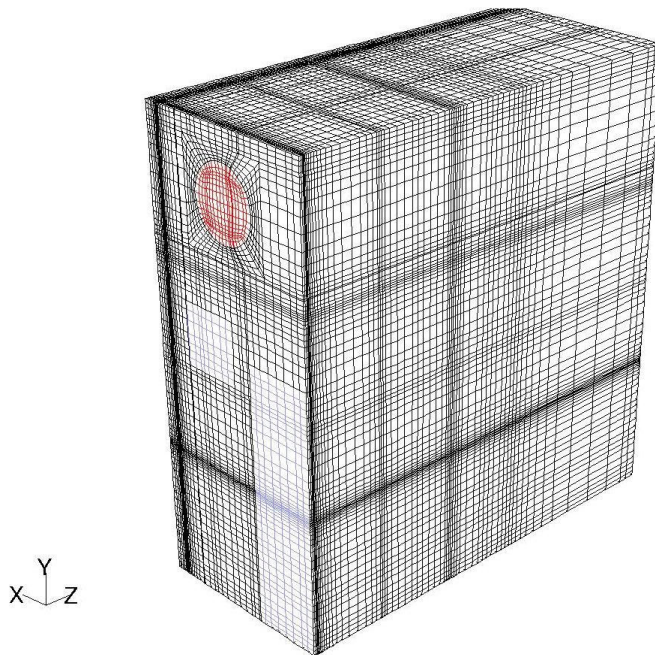


Figure B.1 Grid on computer chassis walls

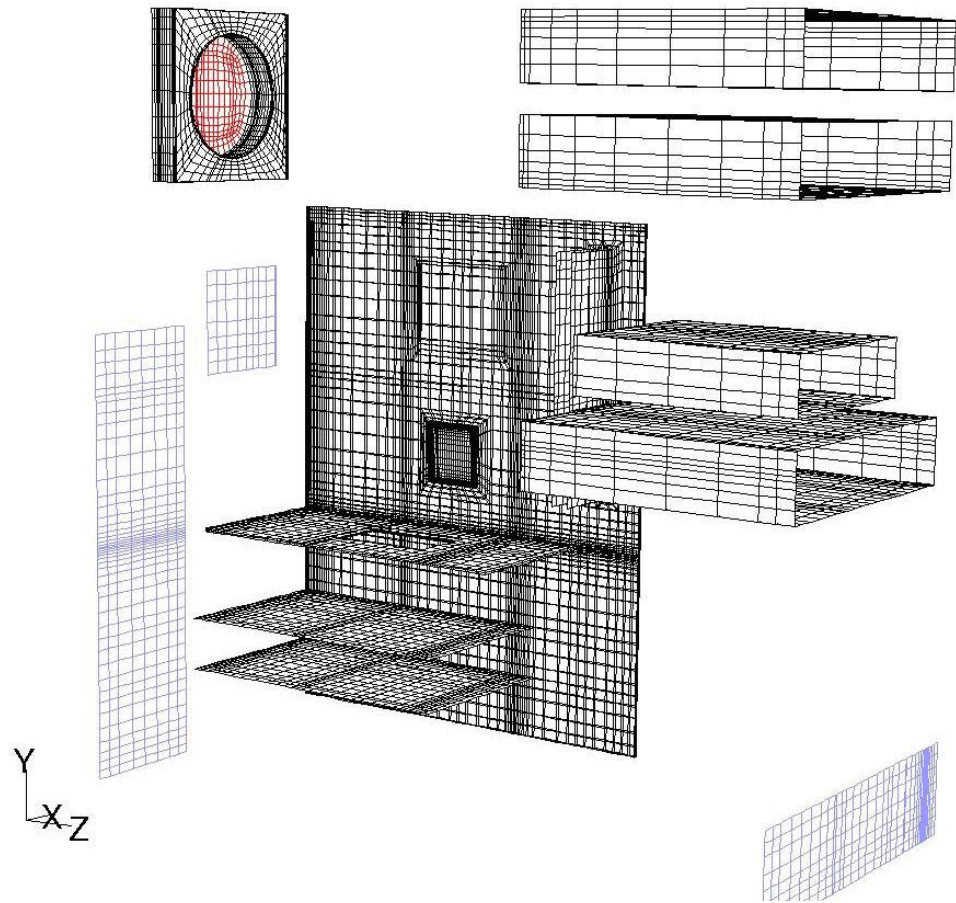


Figure B.2 Mesh of components inside the computer chassis except than the heat sinks.

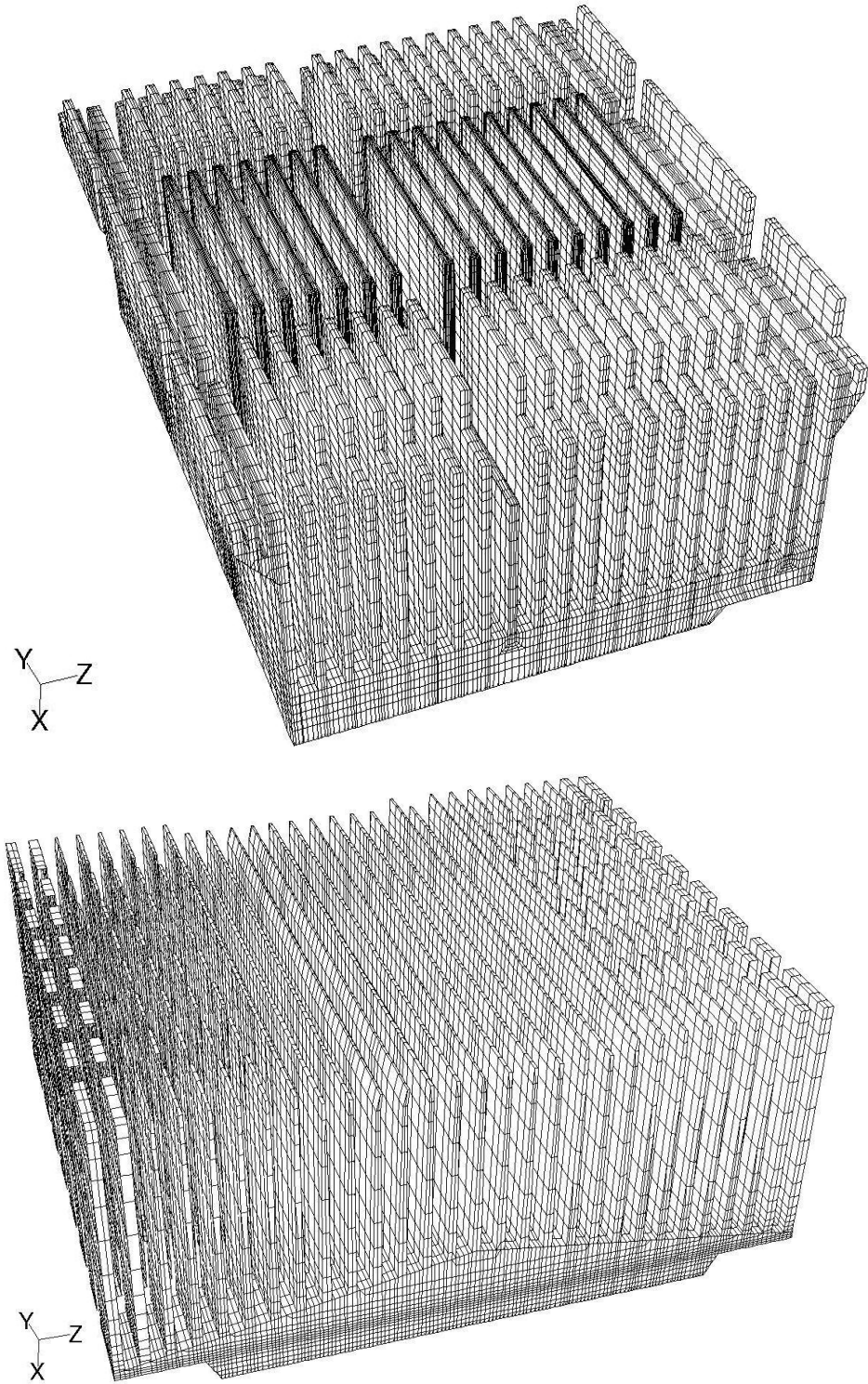


Figure B.3 Surface grid on CPU heat sinks, CoolerMaster at the top and Evercool at the bottom.

It is important to have a good mesh to have an accurate solution. There are some general guidelines to create a good mesh. A good mesh should be fine enough with high quality cells and a good distribution of these cells is essential. Moreover the mesh should not have more cells than the available computer resources can handle. These guidelines are shortly called as rules of QRST, standing for, Quality, Resolution, Smoothness and Total cell count.

Resolution: It is up to the user to choose the resolution of the mesh. But it should be fine enough to capture the most flow features and the solution at the end should be grid independent. A grid independent solution is the one for which a finer grid gives the same results with the original one, and the results do not change as the grid gets finer. The way of checking whether the solution is grid independent or not is to create a grid with more cells to compare the solutions of the two models.

Quality: Icepak determines the quality of cells automatically and when there are cells violating default quality parameters, it is reported. There are three quality parameters checked. One is face alignment; it is the parameter calculating skewness of cells. Elements whose skewness is more than 0.85 are severely distorted and it should be avoided to have such distorted cells in the critical regions. Highly skewed cells not only adversely affect the accuracy but also they may lead to divergence. Face alignment quality is calculated using the minimum, maximum and ideal angles in the cell as shown in Figure B.4. It is defined as;

$$\max\left(\frac{\theta_{\max} - \theta_e}{180 - \theta_e}, \frac{\theta_e - \theta_{\min}}{\theta_e}\right) \quad (\text{B.1})$$

Where, θ_{\max} = largest angle in face

θ_{\min} = smallest angle in face

θ_e = angle for equiangular face



Figure B.4. Maximum and minimum angles in the cell

For ideal elements like square and equilateral triangle, this value is zero.

The second quality parameter is the aspect ratio. It is defined to be the ratio of the largest side of the cell to the smallest side. Cells that are too slender should not be preferred. The third parameter is the volume quality of cells. Extremely small cells may create difficulty in convergence. But when such cells exist, double precision solver may be used.

Smoothness: The good distribution of cells is what the user determines. The number of cells should be more near viscosity affected regions like walls and smaller at non critical regions. Since the critical part of our domain is the heat sink, a finer mesh is generated there. An important point in mesh distribution is that the transition from smaller cells to larger ones should be smooth. The growth rate of the cells from finer mesh to coarser mesh should not exceed 20 % ideally.

Total cell count: The final point in a good mesh is the total number of cells generated. It is vital to have enough number of cells for a good resolution but memory requirements increase as the number of cells increase. Current computer resources do not allow us to solve more than 2 million cells on a single processor on Windows platforms. For our cases, an average of 1 million cells is used.

Due to the complexity of the computer chassis, the fine mesh in and around the heat sink geometry cannot be carried out for the entire model. If it is done, the number of cells exceeds the number, which can be resolved by the available resources, so non-conformal mesh is used. It is “the hanging node mode” for

which the nodes on the two sides of the non-conformal mesh interface do not match each other. Unless there is an abrupt change in the cell size, it is useful to use that kind of mesh to decrease the total cell count. Figure B.5 shows a cut section the mesh in and around the CPU heat sink assembly. Mesh is fine inside the assembly where heat sink is located. The slack between the boundaries and the non-conformal grid interface is 5 mm. Having this slack larger would generate more cells leading to slightly more accurate results.

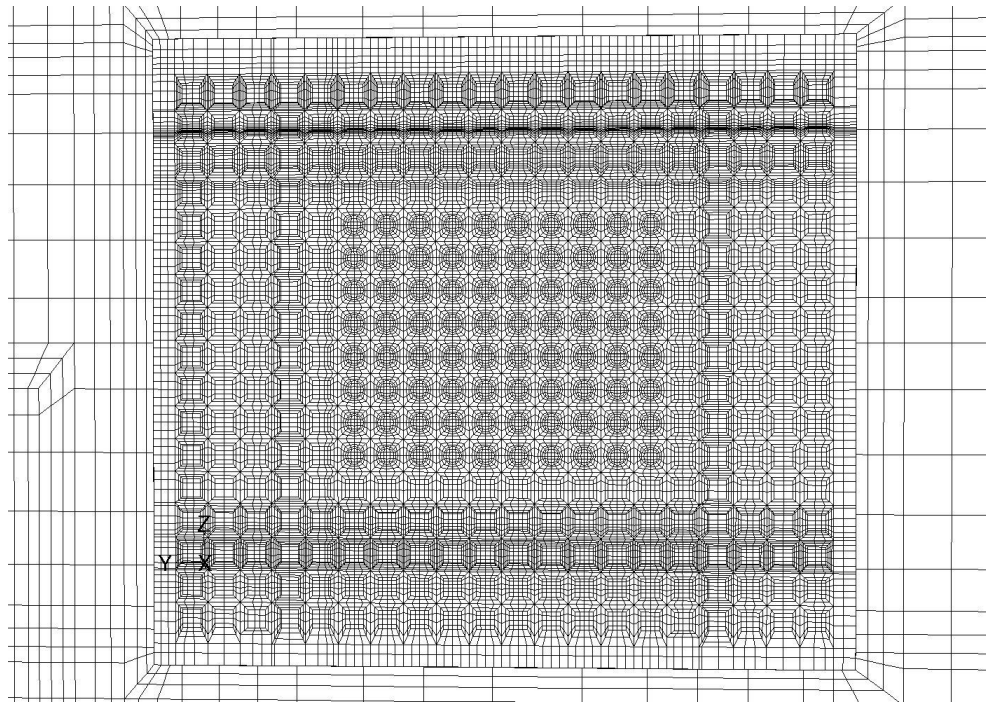


Figure B.5 Non-conformal grid interface

When all the objects are created, the model is ready for meshing. Generally the following procedure is followed for meshing.

- A first cut mesh is generated using the default coarse mesh parameters.
- Mesh quality is examined using surface plots and cut planes. It is important to have at least 4-5 elements on flow boundaries like

grilles and fans. Also at least 3 elements should be placed between the fins of heat sinks. The smoothness of cell distribution and number of cells are the other issues checked.

- For all the cases it is seen that without using assemblies, which are virtual boxes whose inside and outside differ in mesh density, the number of cells exceeded the limit that the available computer resources can solve, even with the default coarse mesh parameters. The reason is the detailed heat sink on the CPU. Therefore heat sinks are put in assemblies and the hanging node mode, i.e. non conformal grid interface, is used for all the cases investigated.
- The default coarse mesh parameters are applied again to create a new mesh. These parameters make sure that there exists at least 2 cells in narrowest air gap and 1 cell across solid blocks. Again the mesh is examined regarding the quality, resolution, smoothness and total cell count. This time, the mesh was far too coarse to resolve the flow features.
- Mesh is refined in regions of high velocity and thermal gradients. Maximum cell size in all directions is constrained to one twentieth of the domain size in order to avoid the very large cells at the corners of the computer chassis.
- Highly skewed cells are generated in some models. It was seen that these cells are generally created in the spaces between the heat sinks and the fans cooling them. The reason is that the fans are circular but the heat sinks are rectangular in fin shapes, so a bad transition occurs from fan to the heat sink in the limited space between them. Therefore additional virtual geometries are placed in those gaps. This is a way to increase the mesh quality in those regions since the user can control the meshing parameters for these additional geometries whereas it is impossible to control the default fluid mesh parameters in all the regions of the domain.

- When the mesh obeys the quality, resolution, smoothness and total cell count parameters; it is ready for the boundary conditions and solution parameters to be defined.

Icepak operates on a “cocooning” methodology when Hexa-Unstructured mesher is used. Each object is meshed as close to the specifications defined as possible. Then, adjacent objects are grouped to generate O-grids for these groups. Cartesian mesh is created for the background, which is the rest of the domain. Finally the mesh of the cut out section around the grouped objects is replaced with an unstructured mesh. Therefore all kind of elements are used in unstructured hexahedral meshing, but since the background mesh and the mesh of the O-grid groups consist of hexahedral elements, most of the cells are hexahedral.

APPENDIX C

FLUENT SOLVER DETAILS

FLUENT solves the governing integral equations for the conservation of mass, momentum, energy and other scalars such as turbulence. A control-volume-based technique is used that consists of following steps [31]:

- A grid is generated on the domain, which is previously explained in preprocessing part.
- For velocity, pressure, temperature and conserved scalars, algebraic sets of equations are constructed by the integration of governing equations on each control volume.
- Discretised equations are linearized and solved iteratively.

The segregated solver is the solution algorithm used by Icepak. For high speed flows another solver, called coupled solver may be activated in FLUENT. Since velocities are very low at electronic cooling processes this method will not be investigated. Using segregated solver approach, the governing equations are solved sequentially (i.e., segregated from one another). Since the governing equations are non-linear (and coupled), many iterations may be done before a converged solution is obtained. Every iteration consists of the steps outlined below:

1. Flow field properties are updated depending on the previous solution. At the first iteration, the properties of the initialized solution will be used.
2. The momentum equations are each solved in turn using current values for pressure and face mass fluxes, in order to update the velocity field.
3. The velocities may not satisfy the continuity equation locally; therefore a pressure correction equation is derived from the continuity equation and momentum equations. This equation is then solved to obtain the

necessary corrections to the pressure and velocity fields and the face mass fluxes so that the continuity is satisfied.

4. Using the previously solved variables, energy and if exists, turbulence and radiation equations are solved.
5. Following these steps a convergence check is done. These steps are continued until the convergence criteria are met. Figure C.1 illustrates the process [31].

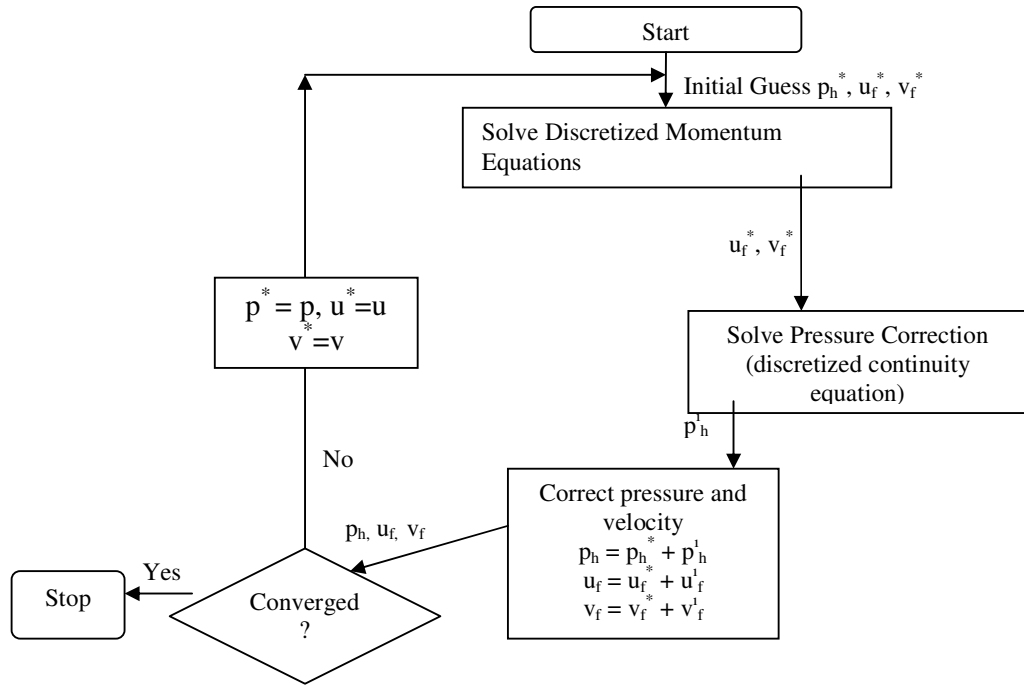


Figure C.1 Simple algorithm

Initial Conditions: Initial velocities and temperatures are defined. Initial pressure is taken to be the ambient pressure. The initialization of the model is important for convergence. If the initial conditions are poor, then it takes longer to converge or it may even result in divergence.

Solution parameters: This is the last step before solution. Number of iterations, convergence criteria, discretization scheme, under-relaxation factors, multi-grid solver parameters and precision solver type are defined.

Number of Iterations: This is the maximum number of iterations done before the solver terminates. In our cases 1000 iterations are requested. If the residuals are still not below the desired values, then additional 1000 iterations are requested.

Convergence Criteria: This is the group of residual values, under which, when the average residuals fall, solver terminates itself. Residuals are the error of the computation. For the matrix $A\phi = Q$, the iterative solution yields an approximate solution ϕ^n which does not satisfy the equation exactly. Instead, there is a non-zero residual ρ^n .

$$A\phi^n = Q - \rho^n \quad (C.1)$$

It is accepted that when the residuals for flow, including continuity, momentum and turbulence parameters fall below 1×10^{-3} and for energy below 1×10^{-7} , the computational error may be ignored. Most of the time, these residuals do not mean much. There have been such cases that although the residuals fell below these values, it was seen that some scalar values have not been converged yet. Therefore, additional convergence monitors are opened. These monitors in our model have always been temperature monitors at the critical parts of our model, namely some arbitrary points on the CPU heat sink. When the temperature values at these monitors converge, it is unnecessary to go further on with the iterations and wait even if the residuals do not fall below the defined convergence criteria. On the other hand, for some models, there is no convergence even when the residuals fell below the convergence criteria. Then the temperature monitors are of great use. The effect of convergence criteria on temperature distribution is investigated.

Discretization scheme: There are first order and second order schemes for pressure, momentum, temperature and if κ - ϵ turbulence model is used, for turbulence kinetic energy and turbulence dissipation rate. A third scheme is available for pressure that is body force weighted. In our models, first order schemes are used for easy convergence. Then iterations are continued with second order schemes for more accurate results.

Under-Relaxation factors: These values have direct impact on convergence. Generally default values are used, but if convergence problems occur, then these values are modified. Decreasing these factors gradually helps convergence. On the other hand, for less computation times they may be increased. These values were decreased before switching to second order schemes to help convergence.

Multi-Grid parameters: Multi-gridding is used in FLUENT in order to speed up convergence. FLUENT uses a point implicit solver which is a Gauss-Seidel scheme. Although the Gauss-Seidel scheme rapidly removes local (high-frequency) errors in the solution, global (low-frequency) errors are reduced at a rate inversely related to the grid size. Thus, for a large number of nodes, the solver “stalls” and the residual reduction rate becomes very low. What multi-grid does is that it coarsens the mesh successively, removes the global error and then refines it back to original. This method is based upon the principle that global (low-frequency) error existing on a fine mesh can be represented on a coarse mesh where it again becomes accessible as local (high-frequency) error: because there are fewer coarse cells overall, the global corrections can be communicated more quickly between adjacent cells [31].

Precision Solver Type: There are single and double precision solvers. On a computer with infinite precision, residuals would go to zero as the solution converges. On an actual computer, the residuals decay to some small value (“round-off”) and then stop changing (“level out”). For single precision computations, residuals can drop as many as six orders of magnitude before hitting round-off. Double precision residuals can drop up to twelve orders of

magnitude. Since we are not after such a high accuracy, single precision solver is used. By this way, we also benefit from the low memory and CPU requirements of the computer.

Linearization:

FLUENT’s segregated solver is an implicit solver. The unknown value for a given variable is computed from a set of linear equations, each of which is written for a single cell in the domain. The unknown variable is related to the known and unknown values from the neighboring cells. Therefore the unknown exists in more than one equation in the system. A point implicit (Gauss-Seidel) linear equation solver is used in conjunction with an algebraic multigrid (AMG) method to solve the resultant set of equations for the dependent variable in each cell. Since there exists one equation per cell, this set of equations is called scalar system of equations. Segregated solver solves for a single variable field in a matrix [31].

The explicit method, for which, the unknown value in each cell is computed using a relation that includes only existing values is not used for our cases.

Discretization:

Finite volume method is used to convert the integral equations to algebraic forms. Steady state conservation equation for a general variable ϕ is used to illustrate the discretization [31]

$$\oint \rho \phi \vec{v} \cdot d\vec{A} = \oint \Gamma_{\phi} \nabla \phi \cdot d\vec{A} + \int_V S_{\phi} dV \tag{C.2}$$

where

ρ = density

\vec{v} =velocity vector

\vec{A} =surface area vector

Γ_ϕ =diffusion coefficient for ϕ

$\nabla\phi$ =gradient of ϕ

S_ϕ =source of ϕ per unit volume

This equation is applied to each control volume in the computational domain.

Discretization of the equation on a given cell yields

$$\sum_f^{N_{faces}} \rho_f \vec{v}_f \phi_f \cdot \vec{A}_f = \sum_f^{N_{faces}} \Gamma_\phi (\nabla\phi)_n \cdot \vec{A}_f + S_\phi V \quad (C.3)$$

where

N_{faces} =number of faces enclosing the cell

ϕ_f =value of ϕ convected through face f

$\rho_f \vec{v}_f \cdot \vec{A}_f$ =mass flux through the face

\vec{A}_f =area of face f

$(\nabla\phi)_n$ =magnitude of $\nabla\phi$ normal to face f

V =cell volume

This is the general form of equations that FLUENT solves, which is applicable to 3D unstructured meshes. Regarding finite volume method, the values of the variable ϕ are stored at the cell centers. However the convective terms in the discretised equation have values of ϕ at the cell faces. Therefore an interpolation scheme is needed to calculate the values at the faces using the values at the cells. This is accomplished using an upwind scheme. FLUENT offers several schemes

for upwinding, first-order upwind, second-order upwind, power law, and QUICK. In our analyses, first-order upwinding is used for first cut analysis and the switch to second-order scheme is done for better accuracy.

The diffusion terms are central-differenced and are always second-order accurate.

A linearized form of discretised equation can be written as

$$a_p \phi = \sum_{nb} a_{nb} \phi_{nb} + b \quad (C.4)$$

where the subscript nb refers to neighbor cells, and a_p and a_{nb} are the linearized coefficients for ϕ and ϕ_{nb} . This kind of equations is written for each cell in the computational grid which results in a set of algebraic equations with a sparse coefficient matrix.

It is desirable to have a control on the change of ϕ . This is typically achieved by under-relaxation, which reduces the change of ϕ at each iteration as follows:

$$\phi = \phi_{old} + \alpha \Delta \phi \quad (C.5)$$

As the under-relaxation factor, α , gets smaller, the new value of ϕ is closer to the one found at the previous iteration. This will increase the convergence possibility. As it gets larger, the change of ϕ is more abrupt. Although it may speed up convergence, there is a higher possibility of divergence.

Discretization of Momentum Equations:

The momentum equation in one direction may be written as

$$a_p u = \sum_{nb} a_{nb} u_{nb} + \sum p_f A_i \hat{i} + S \quad (C.6)$$

by setting $\phi = u$ at the general equation. In this equation pressure values at the faces and face mass fluxes are not known and must be calculated as a part of the solution. For this purpose, pressure interpolation schemes are applied. There are again several schemes in FLUENT for pressure interpolation. Standard, linear, second order, body-force weighted and PRESTO. In our calculations Standard scheme is used. It is suitable for most kind of problems, except for flows with high swirl or high Rayleigh number natural convection flows. The standard scheme works by interpolating the pressure values at the faces using the momentum equation coefficients [31]

If there is a highly swirling flow, or a high Rayleigh number natural convection or very high gradients of pressure among adjacent cells, other methods may be used. In our models, since fans do not create any swirl due to being lumped parameter models and whole case is dominated by forced convection, other pressure interpolation schemes are not preferred.

Pressure-Velocity Coupling

In order to solve the Navier-Stokes equations, pressure field must be known a priori since its gradient contributes to each of the three momentum equations [32]. Furthermore, the continuity equation does not have a dominant variable in incompressible flows. In compressible flows, density is determined from continuity equation and from equation of state, pressure field is calculated. This is not the case for incompressible flows, and one way out of this difficulty is to make-up a pressure field so as to assure the conservation of mass. Several methods like SIMPLE, SIMPLEC, SIMPLER and PISO are available for this purpose. In our calculations the most common one, SIMPLE method, is used.

APPENDIX D

PHYSICAL MODELS

D.1 Turbulence

One of the most challenging tasks in CFD modeling is solving turbulence. All flows are unstable over a certain Reynolds Number, which is the ratio of inertial forces to the viscous forces.

$$\text{Re} = \frac{\rho UL}{\mu} \quad (\text{D.1})$$

At high Reynolds numbers, flows become turbulent and velocity, pressure, temperature and if exists species concentrations vary in all spatial coordinates with a certain degree of randomness.

Turbulent flows are characterized by the following properties:

1. Turbulent flows are time-dependent flows.
2. They are three-dimensional. Fluctuations are in three coordinates. This makes turbulence random and chaotic.
3. They contain a great deal of vorticity. This is one of the principal mechanisms by which the intensity of turbulence increases [32]. The largest turbulent eddies interact with the main flow and extract energy from it by a process called vortex stretching.
4. Turbulence is diffusive. Fluid parcels of different concentrations of at least one of the conserved properties are brought into contact. As a result, heat, mass and momentum are effectively exchanged. This is desired for

heat transfer applications but may not be desired for pumping applications since mixing of momentum results in increased frictional forces [32].

5. Turbulence is dissipative. Since turbulence brings fluids of different momentum into contact, the reduction of the velocity gradients due to the action of viscosity reduces the kinetic energy of the flow [32]. Action of viscosity is especially important for small eddies. Large eddies are dominated by inertia effects and lower viscous effects, so they are effectively inviscid [33]. When small eddies dissipate, this is an irreversible process where lost energy is converted into thermal internal energy [32].

In order to predict turbulence, various methods may be employed. Simple cases may be solved by correlations whereas more complicated ones need the resolution of turbulence equations. There are three major approaches for resolving turbulent equations. Equations may be averaged over time which is called Reynolds Averaged Navier Stokes Equations. This is the most common way in numerical calculations. The second one is Large Eddy Simulation. It solves for the largest scales of the flow while approximating or modeling only the small scales motions. The last method is Direct Numerical Solution for which Navier Stokes equations are solved for all the motions in a turbulent flow.

Although DNS and LES give detailed pictures of the flow, they are far too expensive to perform. Current computer speeds do not allow use of DNS even with very big parallel computing clusters for high Reynolds number flows. Various studies are being conducted on DNS where all of them are very low Reynolds number flows. In order to resolve all the flow features, the cell size forming up the computational grid should be smaller than the smallest eddy. This leads to 100 millions of cells even for flows with Reynolds numbers of several thousand. Also the second aspect making DNS so expensive is the time step size. To capture all eddies of different frequencies; extremely small time step sizes

should be used. Time step size is inversely proportional to Reynolds number. Therefore, DNS has no industrial application at the moment.

LES is also computationally expensive. It may be considered as a compromise between RANS approach and DNS. Large eddies are resolved, whereas smaller ones are modeled. This is sometimes called as filtering. The minimum mesh size determines the eddies to be filtered, i.e., smaller ones are filtered larger ones are solved. Large eddies are generally more energetic and transport conserved properties more effectively. On the other hand, small eddies are weaker and contribute less of these properties. Therefore it makes sense to resolve large eddies and model small ones. Although LES is far less expensive than DNS, it still does not make sense for high Reynolds flows.

Spalart [34] proposes that, if computer speed continues to increase in the fashion as it is today, modeling high Reynolds flows with LES will be feasible only in 2045. The date for DNS is 2080. This makes RANS approach more attractive to fluid engineers.

There are many turbulence models using time averaging. Most popular ones are κ - ϵ models, κ - ω models, Reynolds Stress models, v^2 - f models, Spalart-Allmaras models etc. No single turbulence model is effective and can provide good results for all kind of flows. All of them have advantages and disadvantages. But generally, as the number of equations solved increases, the better the flow field is captured. Spalart-Allmaras is one equation solving turbulence model and it is widely used for aerodynamic applications. κ - ϵ is the one which is the most worked on. There is extensive literature available on κ - ϵ . It has some variants, namely standard κ - ϵ , RNG κ - ϵ , realizable κ - ϵ etc. κ - ω models are better than κ - ϵ for most kind of flows, especially for low-Re Number flows. Its disadvantage is it requires higher density meshes. V^2 - f solves 4 equations and Reynolds Stress Model, RSM, solves 7 equations in 3D. The main advantage of RSM is that it does not use the isotropic eddy viscosity approach whereas all the others do. It is obvious that as the number of equations solved increases, the

computation time increases. Also it is known by experience that, smaller models tend to converge more easily.

D.2 Radiation

FLUENT's surface-to-surface radiation model is used for radiation calculations. As the number of radiating surfaces increases, this model becomes computationally expensive. So only a few models were run with radiation calculations enabled.

Surface-to-surface radiation model in FLUENT is a gray-diffuse model. The main assumption of this model is that any absorption, emission and scattering is ignored, i.e. the exchange of radiative energy between surfaces is virtually unaffected by the medium that separates them. Thus, according to the gray-body model, if a certain amount of radiant energy (E) is incident on a surface, a fraction (ρE) is reflected, a fraction (αE) is absorbed, and a fraction (τE) is transmitted. Since for most applications the surfaces in question are opaque to thermal radiation in the infrared spectrum, the surfaces can be considered opaque. The transmissivity, therefore, can be neglected. It follows, from conservation of energy, that $\alpha + \rho = 1$, since $\alpha = \rho$ (emissivity), and $\rho = 1 - \epsilon$. This assumption is valid for air cooling of electronic devices.

Table D.1 Surface emissivities (Adapted from [8] and [37])

Surface	Emissivity of surfaces (300 K)
Aluminum, polished	0.04
Copper, oxidized	0.76
Fused quartz on aluminum	0.81
White paint on metallic substrate	0.96
Black paint on metallic substrate	0.97